



# A New PWM Strategy Based on a 24-Sector Vector Space Decomposition for a Six-Phase VSI-Fed Dual Stator Induction Motor

Khoudir Marouani, Lotfi Baghli, Djafar Hadiouche, Abdelaziz Kheloui,  
Abderrezak Rezzoug

## ► To cite this version:

Khoudir Marouani, Lotfi Baghli, Djafar Hadiouche, Abdelaziz Kheloui, Abderrezak Rezzoug. A New PWM Strategy Based on a 24-Sector Vector Space Decomposition for a Six-Phase VSI-Fed Dual Stator Induction Motor. IEEE Transactions on Industrial Electronics, 2008, 55 (5), pp.1910-1920. 10.1109/TIE.2008.918486 . hal-03562597

**HAL Id: hal-03562597**

**<https://hal.univ-lorraine.fr/hal-03562597>**

Submitted on 9 Feb 2022

**HAL** is a multi-disciplinary open access archive for the deposit and dissemination of scientific research documents, whether they are published or not. The documents may come from teaching and research institutions in France or abroad, or from public or private research centers.

L'archive ouverte pluridisciplinaire **HAL**, est destinée au dépôt et à la diffusion de documents scientifiques de niveau recherche, publiés ou non, émanant des établissements d'enseignement et de recherche français ou étrangers, des laboratoires publics ou privés.

# A New PWM Strategy Based on a 24-Sector Vector Space Decomposition for a Six-Phase VSI-Fed Dual Stator Induction Motor

Khoudir Marouani, Lotfi Baghli, Djafar Hadiouche, Abdelaziz Kheloui, and Abderrezak Rezzoug

**Abstract**—This paper presents a new space vector pulsewidth modulation (SVPWM) technique for the control of six-phase voltage source inverter (VSI)-fed dual stator induction machines (DSIM). A DSIM is an induction machine which has two sets of three-phase stator windings spatially shifted by 30 electrical degrees and fed by two three-phase VSIs. Despite their advantage of power segmentation, these machines are characterized by large zero sequence harmonic currents, and in particular those of order  $6k \pm 1$ , which are due to the mutual cancellation between the two stator windings. The proposed SVPWM scheme, while easy to implement digitally, reduces significantly these extra stator harmonic currents. Experimental results, collected from a 15 kW prototype machine controlled by a digital signal processor are presented and discussed.

**Index Terms**—Dual stator induction machines (DSIM), six-phase voltage source inverter (VSI), space vector pulsewidth modulation (SVPWM).

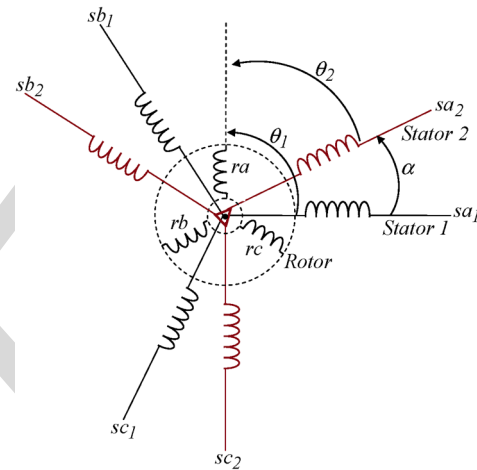


Fig. 1. DSIM windings.

## I. INTRODUCTION

NOWADAYS, electrical machine drives are widely used in industrial applications and transportation systems such as electric/hybrid vehicles, traction locomotives and electric propulsion ships, where high-power levels in conjunction with high-performance requirements are more and more demanded. To achieve these high ratings, there are two possible approaches; one focuses on the converter side by increasing the number of output voltage levels and the other one on the machine side by increasing the number of phases. In the first approach, the idea is to divide the high dc bus voltage into multiple low levels and therefore to distribute the high power required among cells of reduced-voltage power switches without the problem of dynamic voltage sharing encountered in the series connection of active devices. However, increasing the number of inverter levels adds to the control complexity and may introduce some voltage imbalance problems [1]–[3]. It is a solution well suited for high-power and high-voltage utility ap-

plications. For adjustable speed drives, however, an alternative approach is to use a multiphase machine, i.e., a machine with more than three phases in the stator, since the number of phases is not imposed anyway, given that the machine is connected to the electric supply through a dc/ac converter. The number of phases could be used instead as an additional degree of freedom in the overall system design [4].

Although the answer to the question whether it is better to use a multilevel inverter-fed three-phase machine or a multiphase machine depends on the application, it is undeniable that the latter option offers several advantages which may make it appear very attractive. In fact, the most significant features are a low torque ripple, a reduction in the power per phase and fault-tolerance capability. Other interesting advantages can be pointed out, such as a better torque production per ampere for the same machine volume, higher efficiency and improved reliability [5], [6].

A common type of multiphase machine is the dual stator induction machine (DSIM), where two sets of three-phase windings, spatially phase shifted by 30 electrical degrees, share a common stator magnetic core as shown in Fig. 1.

Due to the development of fast switching power semiconductor devices, voltage source inverters (VSIs) are preferred in variable speed machine drives. As VSI-fed multiphase machines are gaining increasing interest for high-power applications, various pulsewidth modulation (PWM) techniques have been developed accordingly, as they strongly affect the overall inverter efficiency and output voltage waveform quality.

Manuscript received February 28, 2007; revised September 24, 2007.

K. Marouani and A. Kheloui are with the Electrical Engineering Laboratory, Polytechnic Military School, 16111 Algiers, Algeria (e-mail: marouani\_khoudir@yahoo.fr; akheloui@caramail.com).

L. Baghli and A. Rezzoug are with the Groupe de Recherche en Electrotechnique et Electronique de Nancy, CNRS UMR 7037, Université Henri Poincaré, 54506 Nancy Cedex, France (e-mail: lotfi.baghli@green.uhp-nancy.fr; abderrezak.rezzoug@green.uhp-nancy.fr).

D. Hadiouche is with the GE Fanuc Automation Solutions Europe, 6468 Echternach, Luxembourg (e-mail: djafar.hadiouche@wanadoo.fr).

Color versions of one or more of the figures in this paper are available online at <http://ieeexplore.ieee.org>.

Digital Object Identifier 10.1109/TIE.2008.918486

In a VSI-fed DSIM, the two stator windings are mutually coupled and small unbalances in the two supply voltages may generate high currents [7]. Furthermore, because of the low impedance seen by the voltage harmonic components generated by the switched voltage waveforms, harmonic currents of high level are circulating uselessly in the two stator windings, adding to the overall losses and therefore to the semiconductor devices ratings [8], [9].

To minimize these extra harmonic currents in a six-phase VSI-fed DSIM, a new 24-sector PWM technique is proposed in this paper and tested on a 15 kW laboratory machine. The digital implementation is carried out on a DS1104 dSPACE controller board. A comparative study between the proposed technique and similar space vector PWM (SVPWM) techniques [5], [10], based on analytical harmonic current analysis, is also developed and discussed.

## II. MACHINE MODEL

The machine model is based on the assumption that space harmonics and magnetic saturation are negligible, and that the two stator three-phase windings are identical and symmetrical with the two neutrals being isolated. In order to derive a practical model suitable for control, a decoupling transformation matrix is used, as proposed in [5]–[7]. The matrix has the following form:

$$[T_s]^{-1} = \frac{1}{\sqrt{3}} \begin{bmatrix} 1 & -\frac{1}{2} & -\frac{1}{2} & \frac{\sqrt{3}}{2} & -\frac{\sqrt{3}}{2} & 0 \\ 0 & \frac{\sqrt{3}}{2} & -\frac{\sqrt{3}}{2} & \frac{1}{2} & \frac{1}{2} & -1 \\ 1 & -\frac{1}{2} & -\frac{1}{2} & -\frac{\sqrt{3}}{2} & \frac{\sqrt{3}}{2} & 0 \\ 0 & -\frac{\sqrt{3}}{2} & \frac{\sqrt{3}}{2} & \frac{1}{2} & \frac{1}{2} & -1 \\ 1 & 1 & 1 & 0 & 0 & 0 \\ 0 & 0 & 0 & 1 & 1 & 1 \end{bmatrix}. \quad (1)$$

By applying (1) to the voltage vector equations, the overall machine model is transformed into three decoupled submodels, written in three independent space coordinates, identified as  $(\alpha-\beta)$ ,  $(x-y)$ , and  $(o_1-o_2)$ , respectively.

The machine voltage submodel in  $(\alpha-\beta)$  coordinates can be written as:

$$\begin{bmatrix} v_{s\alpha} \\ v_{s\beta} \\ v_{r\alpha} \\ v_{r\beta} \end{bmatrix} = \begin{bmatrix} R_s & 0 & 0 & 0 \\ 0 & R_s & 0 & 0 \\ 0 & M\dot{\theta} & R_r & L_r\dot{\theta} \\ -M\dot{\theta} & 0 & -L_r\dot{\theta} & R_r \end{bmatrix} \begin{bmatrix} i_{s\alpha} \\ i_{s\beta} \\ i_{r\alpha} \\ i_{r\beta} \end{bmatrix} + \begin{bmatrix} L_s & 0 & M & 0 \\ 0 & L_s & 0 & M \\ M & 0 & L_r & 0 \\ 0 & M & 0 & L_r \end{bmatrix} \frac{d}{dt} \begin{bmatrix} i_{s\alpha} \\ i_{s\beta} \\ i_{r\alpha} \\ i_{r\beta} \end{bmatrix} \quad (2)$$

where  $\dot{\theta} = \Omega_m$  is the rotor mechanical speed, and  $L_s = L_{ls} + 3L_{ms}$ ,  $L_r = L_{lr} + (3/2)L_{mr}$ ,  $M = (3/\sqrt{2})M_{sr}$ .  $L_{ls}$  and  $L_{lr}$  are the stator and rotor leakage inductances in  $(\alpha-\beta)$  coordinates, respectively.

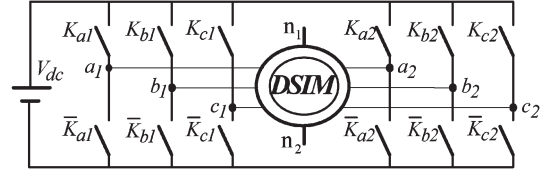


Fig. 2. Six-phase VSI fed DSIM.

The DSIM  $(\alpha-\beta)$  submodel expressed in the stationary reference frame is similar to the three-phase induction machine model [11].

The machine voltage submodel in  $(x-y)$  coordinates is given by:

$$\begin{bmatrix} v_{sx} \\ v_{sy} \end{bmatrix} = \begin{bmatrix} R_s & 0 \\ 0 & R_s \end{bmatrix} \begin{bmatrix} i_{sx} \\ i_{sy} \end{bmatrix} + \begin{bmatrix} L_{lsxy} & 0 \\ 0 & L_{lsxy} \end{bmatrix} \frac{d}{dt} \begin{bmatrix} i_{sx} \\ i_{sy} \end{bmatrix} \quad (3)$$

where  $L_{lsxy}$  is the transformed stator leakage inductance in  $(x-y)$  coordinates.

The machine voltage submodel in  $(o_1-o_2)$  coordinates is expressed as follows:

$$\begin{bmatrix} v_{so1} \\ v_{so2} \\ v_{ro} \end{bmatrix} = \begin{bmatrix} R_s & 0 & 0 \\ 0 & R_s & 0 \\ 0 & 0 & R_r \end{bmatrix} \begin{bmatrix} i_{so1} \\ i_{so2} \\ i_{ro} \end{bmatrix} + \begin{bmatrix} L_{lso} & 0 & 0 \\ 0 & L_{lso} & 0 \\ 0 & 0 & L_{lr} \end{bmatrix} \frac{d}{dt} \begin{bmatrix} i_{so1} \\ i_{so2} \\ i_{ro} \end{bmatrix} \quad (4)$$

where  $L_{lso}$  is the transformed stator leakage inductance in  $(o_1-o_2)$  coordinates.

The electromagnetic torque of the DSIM is expressed only in terms of stator and rotor  $(\alpha-\beta)$  current components, since the  $(x-y)$  and  $(o_1-o_2)$  counterparts do not contribute to the electromechanical energy conversion, as shown by (3) and (4). The expression of the electromagnetic torque is then as follows:

$$T_e = pM(i_{s\beta}i_{r\alpha} - i_{s\alpha}i_{r\beta}) \quad (5)$$

where  $p$  is the number of pole pairs.

## General Remarks

The  $(x-y)$  and  $(o_1-o_2)$  current components do not contribute to the air-gap flux linkages. Hence, they are limited only by the stator resistance and leakage inductance [12], [13]. They produce only losses and therefore must be kept equal to zero or as small as possible.

The transformed voltage equations in the three subframes are well decoupled and, as a result, both machine analysis and control are greatly simplified.

## III. SVPWM CONTROL OF A DOUBLE-STAR INDUCTION MOTOR

The drive system is a six-phase VSI fed DSIM, as shown in Fig. 2. A combinatorial analysis of the inverter switch states shows 64 switching modes. Thus, 64 different voltage vectors can be applied to the machine. Each voltage vector is represented by a decimal number corresponding to the binary number  $(K_{c2}K_{b2}K_{a2}K_{c1}K_{b1}K_{a1})$ , which gives the state of

the upper switches. By using the  $(6 \times 6)$  transformation matrix  $[Ts]^{-1}$ , each voltage vector can be decomposed into  $(\alpha-\beta)$ ,  $(x-y)$ , and  $(o_1-o_2)$  voltages. The  $(o_1-o_2)$  ones are all equal to zero because the neutrals  $(n_1, n_2)$  of the two winding sets are isolated. So the SVPWM strategy operates in two complex planes  $(\alpha-\beta)$  and  $(x-y)$ . Four variables need to be controlled simultaneously during each sampling period, by generating maximum  $(\alpha-\beta)$  and minimum  $(x-y)$  voltage amplitudes. Therefore, during each sampling period, a set of four active voltage vectors must be chosen to fulfil these two conditions, according to the reference voltage vector location. There are numerous ways for choosing such a set.

#### A. Six-Phase SVPWM Techniques

The principle of the PWM control techniques proposed in [5] and [10] is to choose switching sequences in such a way that two consecutive nonzero voltage vectors are practically opposite in phase in the  $(x-y)$  plane. In this way, each change in the applied vectors leads to a sequence of increases and decreases in  $(x-y)$  currents around zero. Moreover, in order to minimize  $(x-y)$  harmonic currents and maintain the lowest switching frequency, there are different choices to allocate zero voltage vectors (0, 7, 56 or 63) within the switching sequences. Thus, the switching sequences presented in [10] lead to continuous and discontinuous modulation techniques and, consequently, to different harmonic distortion characteristics. A modulation technique is continuous when on/off switching occurs within every sampling period, for all inverter legs and all sectors. A modulation technique is discontinuous when one (or more) inverter leg stops switching, i.e., the corresponding phase voltage is clamped to the positive or negative dc bus for at least one sector [14].

#### B. 12-Sector SVPWM Technique

In the SVPWM technique addressed in [5], only the  $(\alpha-\beta)$  voltage vectors having maximum magnitude (45, 41, 9, 11, 27, 26, 18, 22, 54, 52, 36, 37) are employed to synthesize the reference voltage vector  $v_{s\alpha\beta}^*$ . These voltage vectors divide the  $(\alpha-\beta)$  plane into 12 sectors and each sector is  $\pi/6$  rad, as shown in Fig. 3. For example, voltage vectors 45, 41, 9, 11 and 1 are selected when the reference voltage vector is located in sector 1. As shown in Fig. 4, continuous and discontinuous modulation techniques can be obtained according to the switching sequences given below.

1) *Continuous Modulation C6  $\phi$  SVPWM12*: For example, when the reference voltage vector is located in sector 1, a continuous modulation technique (C6  $\phi$  SVPWM12) is obtained with the following sequence:

$$[7-45-41-56-9-11-7|7-11-9-56-41-45-7].$$

2) *Discontinuous Modulation D6  $\phi$  SVPWM12-A*: For the same sector 1, a discontinuous modulation technique (D6  $\phi$  SVPWM12-A) can be obtained with the following sequence:

$$[7-45-41-9-11-7|7-11-9-41-45-7].$$

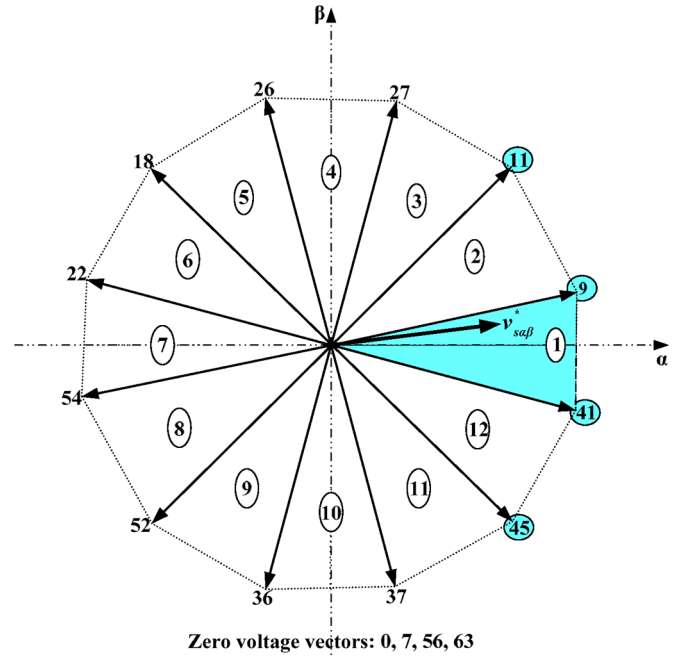


Fig. 3. Presentation of the inverter voltage vectors having maximum magnitude in  $(\alpha-\beta)$  plane.

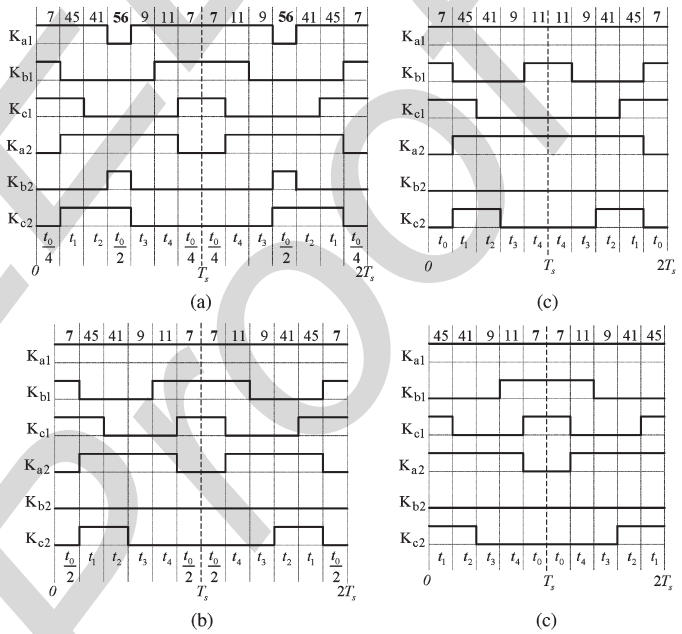


Fig. 4. Twelve-sector SVPWM switching sequences when the reference voltage vector is located in sector 1. (a) C6  $\phi$  SVPWM12. (b) D6  $\phi$  SVPWM12-A. (c) D6  $\phi$  SVPWM12-B1. (d) D6  $\phi$  SVPWM12-B2.

3) *Discontinuous Modulation D6  $\phi$  SVPWM12-B1*: In the D6  $\phi$  SVPWM12-B1, the zero-voltage vectors are applied at the beginning and at the end of the switching sequence as follows:

$$[7-45-41-9-11|11-9-41-45-7].$$

4) *Discontinuous Modulation D6  $\phi$  SVPWM12-B2*: In the D6  $\phi$  SVPWM12-B2, the zero-voltage vectors are applied in the middle of the switching sequence as follows:

$$[45-41-9-11-7|7-11-9-41-45].$$



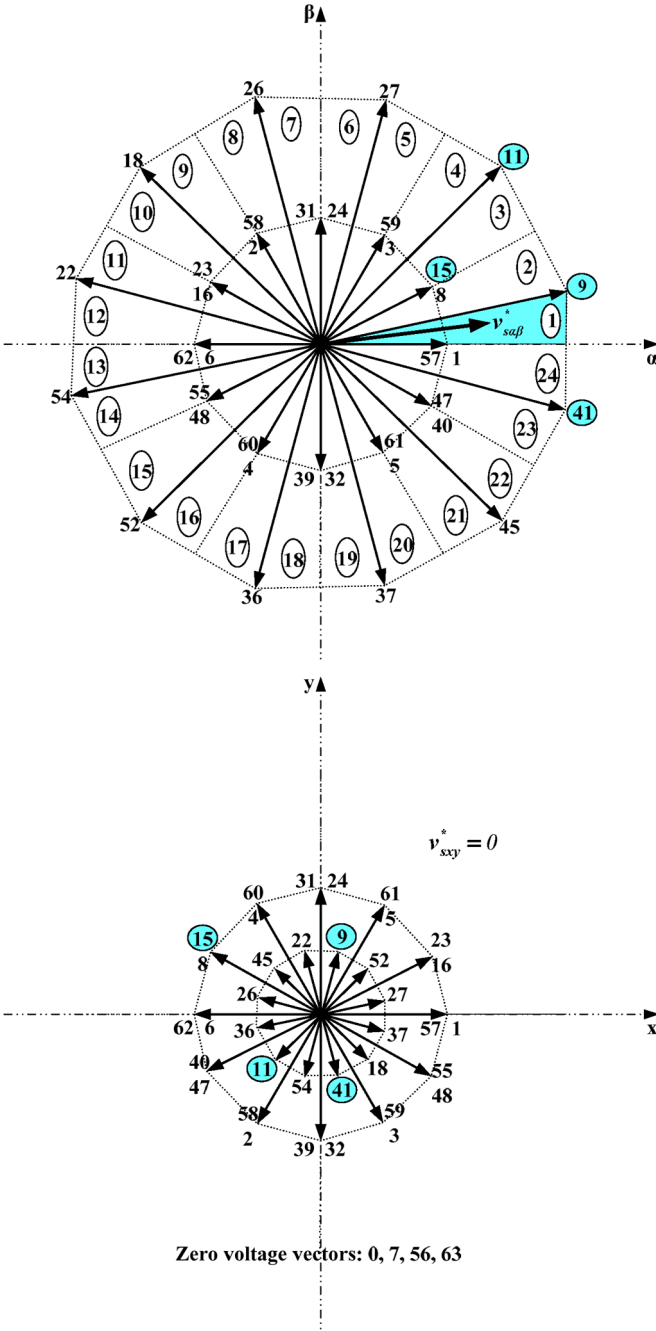


Fig. 5. Presentation of the inverter voltage vectors having maximum and half magnitude in  $(\alpha-\beta)$ , and  $(x-y)$  planes.

### 191 C. Proposed 24-Sector SVPWM Technique

192 As shown in Fig. 4, the switching pattern corresponding  
193 to the switching sequences of the 12-sector PWM techniques  
194 presents asymmetrical waveforms and usually more than two  
195 transitions (from low to high or from high to low) occur on  
196 the corresponding PWM outputs within a sampling period,  
197 which increases the switching frequency of the inverter legs  
198 and causes difficulties for digital signal processor (DSP) im-  
199 plementation of these strategies. Accordingly, some additional  
200 adaptations in DSP programs are necessary to ensure successful  
201 experiments [15], [16].

202 To overcome these drawbacks, the new 24-sector SVPWM  
203 technique proposed in this paper combines the maximum

magnitude  $(\alpha-\beta)$  voltage vectors and the ones with half  
204 magnitude (1, 57, 8, 15, 3, 59, 24, 31, 2, 58, 16, 23, 6, 205  
62, 48, 55, 4, 60, 32, 39, 5, 61, 40, 47) generated by one  
206 inverter. These voltage vectors divide the  $(\alpha-\beta)$  plane into  
207 twenty four  $\pi/12$ -rad sectors, as shown in Fig. 5. In each  
208 sampling period, the reference voltage vector is achieved by  
209 selecting a set of three voltage vectors among those having  
210 maximum magnitude and a fourth vector among the ones with  
211 half magnitude. For example, voltage vectors 41, 9, 11 and 15  
212 are selected when the reference voltage vector is located in  
213 sector 1. Then, the voltage vectors applying times:  $t_1, t_2, t_3$  and  
214  $t_4$  are obtained as explained in Appendix A. For the remaining  
215 time  $t_0 = T_s - (t_1 + t_2 + t_3 + t_4)$ , zero state vectors (0, 7, 56  
216 or 63) are applied. Consequently, simple PWM outputs with  
217 symmetrical waveforms are obtained. As shown in Fig. 6,  
218 only two transitions or less (from low to high or from high  
219 to low) occur on the corresponding PWM outputs within a  
220 sampling period. This fact decreases the switching frequency  
221 of the inverter legs and allows easy DSP implementation. The  
222 switching sequences and the corresponding applying times for  
223 all sectors are presented in Table I. It should also be noticed  
224 that both continuous and discontinuous modulation techniques  
225 can be obtained with this new 24-sector SVPWM scheme. This  
226 is achieved by selecting the appropriate zero voltage vector  
227 locations within the switching sequence.

228  
229 1) *Continuous Modulation C6  $\phi$  SVPWM24*: Continuous  
230 PWM technique (C6  $\phi$  SVPWM24) can be obtained for all sec-  
231 tors by selecting the switching sequences presented in Table I.  
232 As an example, when the reference voltage vector is located  
233 in sector 1, a C6  $\phi$  SVPWM24 is obtained by selecting the  
234 following sequence:

$$|56-41-9-11-15-7|7-15-11-9-41-56|.$$

235 2) *Discontinuous Modulation D6  $\phi$  SVPWM24-B1 and B2*:  
236 Two discontinuous PWM schemes can be obtained through the  
237 appropriate positioning of the zero voltage vectors. In sector 1,  
238 the examples are as follows.

239 1) *D6  $\phi$  SVPWM24-B1*: The first discontinuous modulation  
240 technique can be obtained by placing the zero voltage  
241 vector both at the beginning and at the end of the switch-  
242 ing sequence, as follows:

$$|56-41-9-11-15|15-11-9-41-56|.$$

243 2) *D6  $\phi$  SVPWM24-B2*: The second discontinuous mod-  
244 ulation technique is obtained by placing the zero volt-  
245 age vector in the middle of the switching sequence, as  
246 follows:

$$|41-9-11-15-7|7-15-11-9-41|.$$

247 3) *Switching Sequences and Applying Time Selection*: For  
248 optimal DSP implementation and low algorithm execution time,  
249 the applying times ( $t_1, t_2, t_3$ , and  $t_4$ ) computation can be  
250 simplified by an offline calculation for all sectors in the same  
251 manner as for sector 1. As a result, within each sampling period,  
252 there is a total of only 12 coefficients  $T_i$  to be calculated in (6).

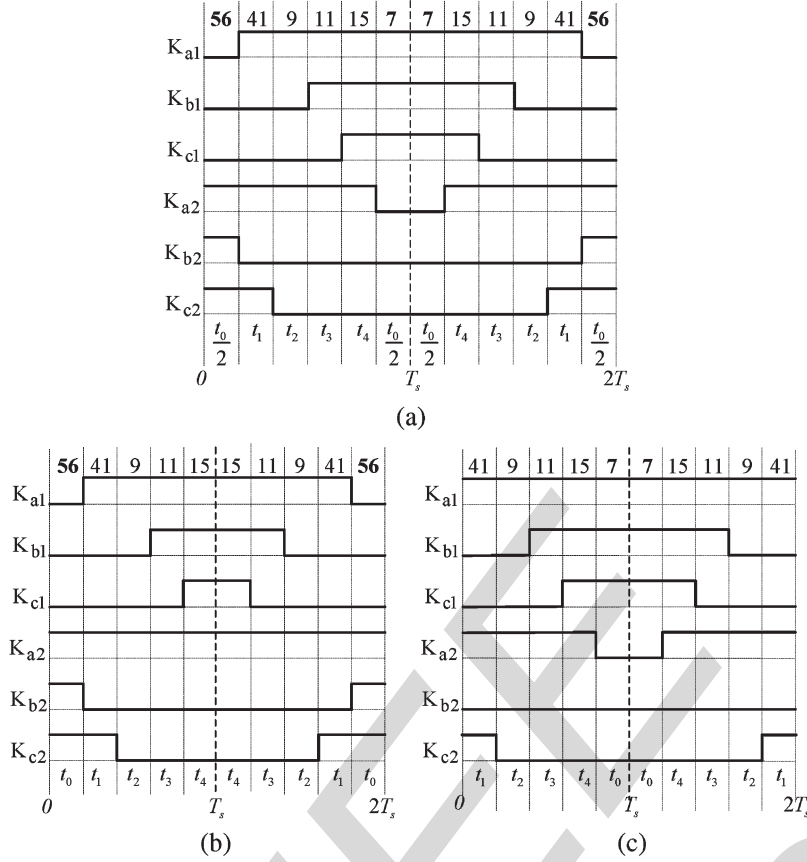


Fig. 6. Twenty-four-sector SVPWM switching sequences when the reference voltage vector is located in sector 1. (a) C6  $\phi$  SVPWM24. (b) D6  $\phi$  SVPWM24-B1. (c) D6  $\phi$  SVPWM24-B2.

Table I describes the C6  $\phi$  SVPWM24 switching sequences and applying time selection according to the sector number in the  $(\alpha-\beta)$  plane.

0.907, coincides with the corresponding value for the three-phase SVPWM [20]. Note that  $m_{\max}$  is obtained by solving  $t_0 = T_s - (t_1 + t_2 + t_3 + t_4) = 0$  as shown in Appendix B.

$$\begin{bmatrix} T_1 \\ T_2 \\ T_3 \\ T_4 \\ T_5 \\ T_6 \\ T_7 \\ T_8 \\ T_9 \\ T_{10} \\ T_{11} \\ T_{12} \end{bmatrix} = \frac{T_s}{2V_{dc}} \begin{bmatrix} \sqrt{3}-2 & 1 \\ 1 & -\sqrt{3} \\ 1 & \sqrt{3}-2 \\ 0 & 2 \\ \sqrt{3}-1 & \sqrt{3}-1 \\ -(\sqrt{3}-1) & \sqrt{3}-1 \\ \sqrt{3} & -1 \\ 1 & -(\sqrt{3}-2) \\ -(\sqrt{3}-2) & 1 \\ 2 & 0 \\ \sqrt{3} & 1 \\ 1 & \sqrt{3} \end{bmatrix} \begin{bmatrix} v_{s\alpha}^* \\ v_{s\beta}^* \end{bmatrix}. \quad (6)$$

#### D. Maximum Modulation Index

The modulation index  $m$  can be defined as the ratio of the fundamental component magnitude of the line to neutral inverter output voltage  $V_{1m}$  to the fundamental component magnitude of the six-step mode voltage  $V_{1m6step} = 2V_{dc}/\pi$  [17]. When the inverter is operating in the linear modulation region, the sum of the applying times of the active voltage vectors is less than the switching period  $T_s$  [18], [19]. The largest value for linear output with the 12-sector and the proposed 24-sector SVPWM techniques,  $m_{\max} = \pi/(2\sqrt{3}) \approx$

#### IV. HARMONIC CURRENT ANALYSIS

The voltage and current waveform quality of the PWM-VSI drives is determined via the switching frequency harmonics, since they determine the switching frequency copper losses and the torque ripple of a motor load and the line current total harmonic distortion of a line-connected VSI. While the copper losses are measured over a fundamental cycle and therefore require a per fundamental cycle (macroscopic) rms ripple current value calculation, the peak and local stresses are properly investigated on a per-carrier cycle (microscopic) basis. Therefore, first a microscopic and then a macroscopic investigation is required [20]. Because, the machine model includes  $(\alpha-\beta)$  and  $(x-y)$  components, the harmonic current analysis must be made for the  $(\alpha-\beta)$  and  $(x-y)$  currents.

##### A. Normalized Harmonic Currents and Fluxes Calculation

The stator voltage equations in the stator coordinate system are expressed as follows:

$$\begin{aligned} v_{s\alpha\beta} &= R_s i_{s\alpha\beta} + \frac{d\lambda_{s\alpha\beta}}{dt} \\ v_{sxy} &= R_s i_{sxy} + L_{lsxy} \frac{di_{sxy}}{dt} \end{aligned} \quad (7)$$

TABLE I  
PROPOSED C6  $\phi$  SVPWM24 SWITCHING SEQUENCES

Sector	Switching sequences	Voltage vectors applying times			
		$t_1$	$t_2$	$t_3$	$t_4$
1	56-41-9-11-15-7	$T_2$	$T_5$	$T_4$	$-T_1$
2	56-57-41-9-11-7	$T_1$	$T_2$	$T_3$	$T_4$
3	0-9-11-27-59-63	$T_7$	$T_9$	$-T_2$	$-T_6$
4	0-8-9-11-27-63	$T_6$	$T_7$	$T_8$	$-T_2$
5	7-11-27-26-24-56	$T_{10}$	$T_1$	$-T_7$	$T_3$
6	7-3-11-27-26-56	$-T_3$	$T_{10}$	$T_5$	$-T_7$
7	63-27-26-18-2-0	$T_{11}$	$T_6$	$-T_{10}$	$T_8$
8	63-31-27-26-18-0	$-T_8$	$T_{11}$	$T_9$	$-T_{10}$
9	56-26-18-22-23-7	$T_{12}$	$-T_3$	$-T_{11}$	$T_5$
10	56-58-26-18-22-7	$-T_5$	$T_{12}$	$T_1$	$-T_{11}$
11	0-18-22-54-62-63	$T_4$	$-T_8$	$-T_{12}$	$T_9$
12	0-16-18-22-54-63	$-T_9$	$T_4$	$T_6$	$-T_{12}$
13	7-22-54-52-48-56	$-T_2$	$-T_5$	$-T_4$	$T_1$
14	7-6-22-54-52-56	$-T_1$	$-T_2$	$-T_3$	$-T_4$
15	63-54-52-36-4-0	$-T_7$	$-T_9$	$T_2$	$T_6$
16	63-55-54-52-36-0	$-T_6$	$-T_7$	$-T_8$	$T_2$
17	56-52-36-37-39-7	$-T_{10}$	$-T_1$	$T_7$	$-T_3$
18	56-60-52-36-37-7	$T_3$	$-T_{10}$	$-T_5$	$T_7$
19	0-36-37-45-61-63	$-T_{11}$	$-T_6$	$T_{10}$	$-T_8$
20	0-32-36-37-45-63	$T_8$	$-T_{11}$	$-T_9$	$T_{10}$
21	7-37-45-41-40-56	$-T_{12}$	$T_3$	$T_{11}$	$-T_5$
22	7-5-37-45-41-56	$T_5$	$-T_{12}$	$-T_1$	$T_{11}$
23	63-45-41-9-1-0	$-T_4$	$T_8$	$T_{12}$	$-T_9$
24	63-47-45-41-9-0	$T_9$	$-T_4$	$-T_6$	$T_{12}$

where the stator and the rotor flux equations are given by:

$$\begin{aligned}\lambda_{s\alpha\beta} &= L_s i_{s\alpha\beta} + M i_{r\alpha\beta} \\ \lambda_{r\alpha\beta} &= L_r i_{r\alpha\beta} + M i_{s\alpha\beta}.\end{aligned}\quad (8)$$

The stator flux equation can be rewritten as:

$$\lambda_{s\alpha\beta} = \sigma L_s i_{s\alpha\beta} + \frac{M}{L_r} \lambda_{r\alpha\beta}. \quad (9)$$

Substituting (9) in (7), the stator voltage equation can be expressed as follows:

$$v_{s\alpha\beta} = R_s i_{s\alpha\beta} + \sigma L_s \frac{di_{s\alpha\beta}}{dt} + \frac{M}{L_r} \frac{d\lambda_{r\alpha\beta}}{dt}. \quad (10)$$

If only the harmonic voltages and currents are considered, it will be assumed that the reference voltage vector  $v_{s\alpha\beta}^*$  is constant over the switching period  $T_s$ , because the switching frequency  $f_s$  is much higher than the fundamental frequency  $f_e$ , and that the stator and the rotor time constants are much larger than the switching period, with the resistance drops being neglected [21]. Under these assumptions, the voltages and

currents can be separated in the harmonic components, which change over  $T_s$  while the fundamental components remain constant over the same period. Thus, from (7) and (10), the harmonic voltage equations can be expressed as follows:

$$\begin{aligned}\tilde{v}_{s\alpha\beta} &= \sigma L_s \frac{d\tilde{i}_{s\alpha\beta}}{dt} \\ \tilde{v}_{sxy} &= L_{lsxy} \frac{d\tilde{i}_{sxy}}{dt}\end{aligned}\quad (11)$$

where  $\tilde{v}_{s\alpha\beta}$  is the harmonic voltage and is equal to the difference between the actual voltage vector and the reference vector  $v_{s\alpha\beta}^*$ .

Assuming that the instantaneous harmonic currents are zero at the beginning and at the end of the carrier cycle, the  $(\alpha-\beta)$  and  $(x-y)$  harmonic stator currents per-carrier cycle can be calculated as follows [20], [22], [23]:

$$\begin{aligned}\tilde{i}_{s\alpha\beta} &= \frac{1}{\sigma L_s} \int_{NT_s}^{(N+1)T_s} (V_{s\alpha\beta k} - v_{s\alpha\beta}^*) dt \\ \tilde{i}_{sxy} &= \frac{1}{L_{lsxy}} \int_{NT_s}^{(N+1)T_s} (V_{sxy k}) dt.\end{aligned}\quad (12)$$

In (12),  $V_{s\alpha\beta k}$  and  $V_{sxy k}$  are the inverter output voltage vectors of the  $k$ th state. They change according to the selected switching sequence, since for high  $f_s/f_e$  values, the  $v_{s\alpha\beta}^*$  term can be assumed as constant within a carrier cycle. Thus, the above integral can be calculated in a closed form.

Because the harmonic current and harmonic flux are only different in scale, and in order to eliminate the need for load parameters in (12), the harmonic flux trajectories can be investigated. Nevertheless, the  $(x-y)$  current components are limited by the stator leakage inductance  $L_{lsxy}$ , which depends on the coil pitch of the stator windings [10]. Consequently, the harmonic characteristics of the VSI feeding DSIM should be investigated with the introduction of the coefficient  $k_{\sigma xy} = \sigma L_s / L_{lsxy}$ , which is necessary to evaluate and compare the performances of the PWM techniques. So, employing (12) and normalizing with respect to  $\lambda_b$ , the per-carrier cycle rms value of the normalized harmonic current can be calculated with:

$$\begin{aligned}\tilde{i}_{srms}^2(m, \theta) &= \left(\frac{\lambda_b}{\sigma L_s}\right)^2 \frac{1}{T_s} \int_{NT_s}^{(N+1)T_s} (\tilde{\lambda}_{s\alpha\beta}^2 + k_{\sigma xy}^2 \tilde{\lambda}_{sxy}^2) dt \\ &= \left(\frac{\lambda_b}{\sigma L_s}\right)^2 (\tilde{\lambda}_{s\alpha\beta rms}^2(m, \theta) + k_{\sigma xy}^2 \tilde{\lambda}_{sxy rms}^2(m, \theta)) \\ &= \left(\frac{\lambda_b}{\sigma L_s}\right)^2 (\tilde{\lambda}_{srms}^2(m, \theta))\end{aligned}\quad (13)$$

where  $\lambda_b = 2\sqrt{3}V_{dc}T_s/\pi$ ,  $\tilde{\lambda}_{s\alpha\beta} = \sigma L_s \tilde{i}_{s\alpha\beta}$ , and  $\tilde{\lambda}_{sxy} = L_{lsxy} \tilde{i}_{sxy}$

TABLE II  
SWITCHING FREQUENCY REDUCTION COEFFICIENT

N°	SVPWM Techniques	$k_f$	$f_s$
1	C6 $\phi$ SVPWM12	1	$f_s = \frac{1}{k_f} \cdot f_{sw}$
2	D6 $\phi$ SVPWM12-A	2/3	
3	D6 $\phi$ SVPWM12-B1	1/2	
4	D6 $\phi$ SVPWM12-B2	5/12	
5	C6 $\phi$ SVPWM24	1	
6	D6 $\phi$ SVPWM24-B1	5/6	
7	D6 $\phi$ SVPWM24-B2	2/3	

The per-fundamental cycle rms value of the harmonic current determines the waveform quality and harmonic losses. Averaging (13) over a fundamental period results in the global harmonic current calculation as follows:

$$\begin{aligned}
 \tilde{I}_{sfrms}^2(m) &= \left( \frac{\lambda_b}{\sigma L_s} \right)^2 \frac{1}{2\pi} \int_{2\pi} \tilde{\lambda}_{sfrms}^2(m, \theta) d\theta \\
 &= \left( \frac{\lambda_b}{\sigma L_s} \right)^2 \left( \tilde{\lambda}_{s\alpha\beta frms}^2(m) + k_{\sigma xy}^2 \tilde{\lambda}_{sxy frms}^2(m) \right) \\
 &= \left( \frac{\lambda_b}{\sigma L_s} \right)^2 \tilde{\lambda}_{sfrms}^2(m). \quad (14)
 \end{aligned}$$

The above integral yields a polynomial function of the modulation index  $m$ . As an example, the per-fundamental cycle rms normalized harmonic flux  $\tilde{\lambda}_{sfrms}$  was calculated for all the discussed PWM techniques. This results in  $m$  dependent analytical formulas summarized in Appendix C.

#### B. Performance Comparison

For comparison purposes, the harmonic current analysis is performed at the same average switching frequency  $f_{sw}$  for all the PWM techniques. Therefore, a switching frequency reduction coefficient  $k_f$  is introduced for each PWM technique according to Table II. This coefficient can be determined from the ratio of the discontinuous to the continuous PWM techniques regarding the number of commutations of all legs during one sampling period. The curves of the per-fundamental cycle normalized rms harmonic flux for all the discussed PWM techniques have been plotted as a function of modulation index  $m$ , as shown in Fig. 7. It is clear that the rms value of the harmonic flux varies with the PWM technique used and according to the selected switching sequences. These curves show that the D6  $\phi$  SVPWM12-A has practically the best performance at a low modulation index range, while the D6  $\phi$  SVPWM12-B1-B2 exhibits the best performance in the high modulation index range. However, as the modulation index increases, the C6  $\phi$  SVPWM12 performance rapidly degrades compared to the C6  $\phi$  SVPWM24 of the proposed 24-sector PWM scheme, which reveals excellent performance over the whole voltage range. While the D6  $\phi$  SVPWM24-B1-B2 PWM strategies present harmonic characteristics similar to the ones obtained with the D6  $\phi$  SVPWM12-A-B1 and B2 strategies, the

proposed 24-sector PWM techniques allow a sampling frequency increase and as a result, the switching frequency can be increased by a factor of two as compared to the 12-sector PWMs. Therefore, significant harmonic current reductions can be achieved as shown in Fig. 7(h) for the worst case, when  $k_{\sigma xy} = 10$ .

It should be noted that discontinuous PWM techniques allow a higher sampling rate selection and can be applied in a high voltage range, while continuous ones are advantageous in the low voltage range. In addition, an optimal PWM scheme can be obtained with a transition between these SVPWM strategies to allow rms harmonic current minimization over the whole voltage range. The intersection points define the optimal transition between different PWM techniques.

Finally, a careful look at D6  $\phi$  SVPWM12-B1 in Fig. 4(c) shows that during one switching period  $T_s$ , two inverter legs have commutations twice. D6  $\phi$  SVPWM12-B2 in Fig. 4(d) shows that one inverter leg has commutations twice. This is never the case for D6  $\phi$  SVPWM24-B1 and B2. Therefore, 12-sector discontinuous PWMs have a maximum instantaneous switching frequency twice as big as in the case of 24-sector discontinuous PWMs. This fact has an impact on inverter switching losses [14], [20]. While it is not the aim of this paper to evaluate the performance of PWM techniques in terms of inverter switching and conduction losses, it can be expected that the 24-sector discontinuous PWMs will have a better performance than the 12-sector ones. Further works on switching and conduction losses are in progress and will be reported in a subsequent paper.

## V. EXPERIMENTAL RESULTS

To confirm the feasibility of the proposed SVPWM techniques over the entire voltage range under  $V/f$  control, a set of experiments are carried out. The experimental test bench (Fig. 8) is composed of a six-phase VSI feeding a 15 kW DSIM prototype, and the whole control algorithm is tested on a dSPACE DS1104 controller board. The original 320F240 firmware does not allow the change in PWM compare registers and action registers many times during a period. So, to allow four changes within PWM period  $T_s$ , the flashed firmware is reprogrammed [15], [24]. Hence, it is possible to implement the 12-sector PWM techniques.

On the contrary, for the proposed 24-sector PWM strategies, usually at most two transitions (from low to high or from high to low) occur symmetrically on the corresponding PWM outputs within a sampling period. This allows easier DSP implementation. Then the original 320F240 firmware is used with the help of specially developed user functions that allow the synchronization of six full PWM and three simple PWM simultaneously on the DS1104 DSP board.

These PWM techniques are successfully tested and the following conclusions can be drawn from these experimental results: In the case of the 12-sector PWM strategies, usually more than two transitions (from low to high or from high to low) occur on the corresponding PWM outputs. This increases the switching frequency of the inverter legs and complicates the experimental test. However, the number of transitions



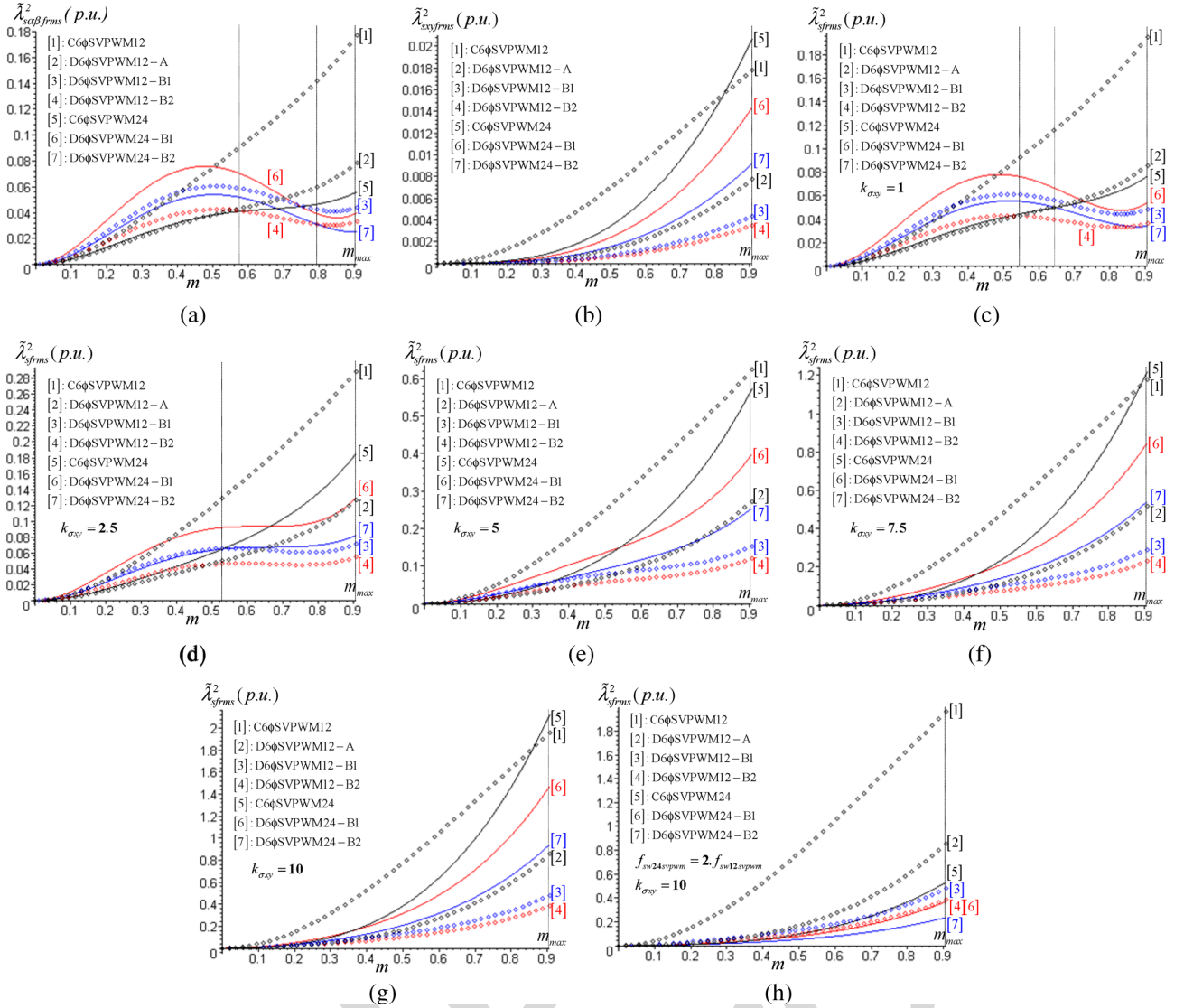


Fig. 7. Per fundamental cycle normalized rms harmonic flux as a function of modulation index  $m$ , for all the discussed PWM techniques. (a)  $(\alpha-\beta)$  rms harmonic flux. (b)  $(x-y)$  rms harmonic flux. (c), (d), (e), (f), (g) RMS harmonic flux at different leakage coupling ( $k_{\sigma xy} = 1; 2.5; 5; 7.5; 10$ ), at the same average switching frequency  $f_{sw}$ . (h) RMS harmonic flux with  $k_{\sigma xy} = 10$ , at  $f_s = 2 \cdot f_{sw}$  for the proposed 24-sector PWM techniques.

on the corresponding PWM outputs is reduced in the case of the proposed 24-sector PWM strategies, which decrease the switching frequency of the inverter legs and allow easy DSP implementation. In addition, for discontinuous PWM techniques, at least two PWM outputs remain unchanged during the entire sampling period. Therefore, the carrier frequency can be increased with harmonic losses reduction.

Experimental results under constant  $V/f$  control, for the cases of C6  $\phi$  SVPWM12, D6  $\phi$  SVPWM12-B2, C6  $\phi$  SVPWM24, and D6  $\phi$  SVPWM24-B2 techniques are presented in Fig. 9. The average switching frequency is set to  $f_{sw} = 5$  kHz and the motor is running at 735 r/min with a connected load. As expected, these SVPWM techniques allow the control of the  $(\alpha-\beta)$  and  $(x-y)$  current components simultaneously.

However, these experimental results demonstrate that the continuous PWM techniques produce a larger amplitude of the harmonic currents in the  $(x-y)$  plane as compared to the discontinuous ones where the amplitude of these currents

is minimized. Moreover, the phase current presents a pure sinusoidal shape and the trajectory of the  $(\alpha-\beta)$  stator current components is a circle for all these PWM techniques, confirming that these currents are controlled as well as  $(x-y)$  harmonic currents. Indeed, it should be remembered that the carrier frequency can be increased by a factor of two for a 50% reduction of harmonic losses in the case of C6  $\phi$  SVPWM24, or by a factor three for a 66% reduction in harmonic losses with the D6  $\phi$  SVPWM24-B2 technique. In addition, due to the simplicity and regularity of the proposed 24-sector PWM techniques, low-cost DSPs for motor control may easily be used.

## VI. CONCLUSION

In this paper, a new SVPWM technique based on the vector space decomposition suitable for six-phase VSI-fed DSIM has been presented. The switching sequences presented lead to continuous and discontinuous modulation strategies, according

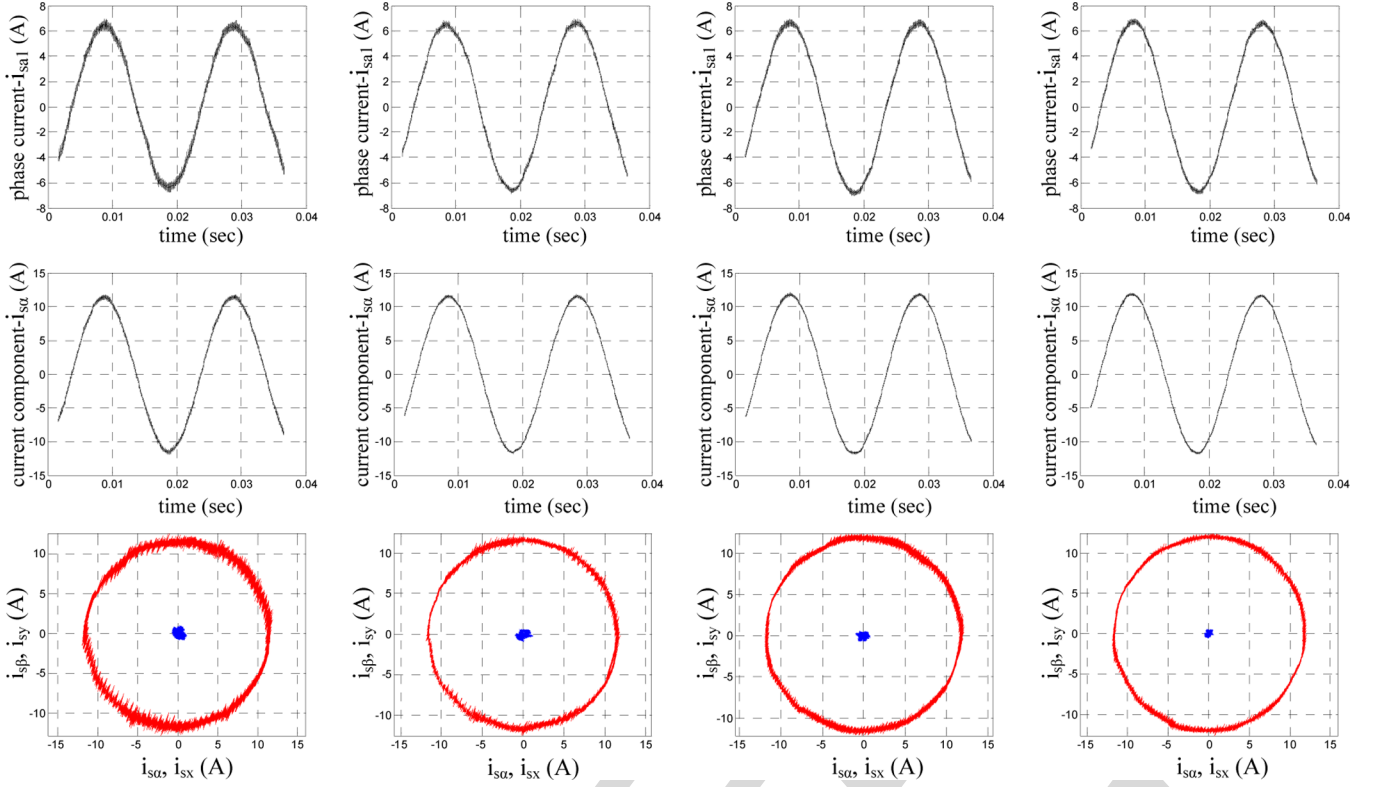


Fig. 8. Experimental test bench.

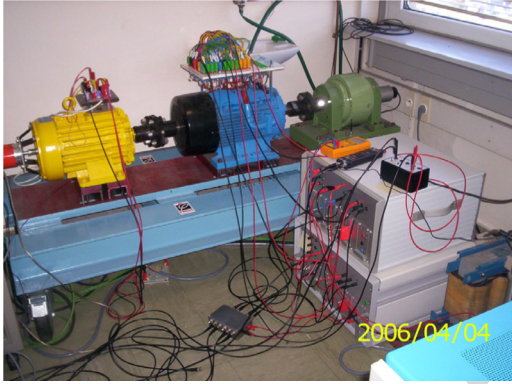


Fig. 9. Experimental results of the SVPWM techniques with the motor operating under a constant  $V/f$  control with connected load for  $f_e = 50$  Hz, at 735 r/min and for the same average switching frequency  $f_{sw}$ . From top to bottom:  $i_{sa1}$  phase current,  $i_{s\alpha}$  current component,  $(\alpha-\beta)$  and  $(x-y)$  plane current trajectories. From left to right: C6  $\phi$  SVPWM12, D6  $\phi$  SVPWM12-B2, C6  $\phi$  SVPWM24, and D6  $\phi$  SVPWM24-B2.

453 to the position of zero voltage vectors during each sampling  
454 period. It is shown that the harmonic current rms values vary  
455 according to the selected switching sequence and the voltage  
456 range. Likewise, from this point of view, the continuous PWM  
457 technique has an advantage in the low and medium voltage  
458 range, while the discontinuous PWM strategy is advantageous  
459 in the high voltage range. Thus, the combination of these  
460 strategies provides the best harmonic current performance over  
461 the whole voltage range. It has been demonstrated that the pro-  
462 posed 24-sector SVPWM techniques, while easy to implement  
463 digitally, allow a switching frequency increase with significant  
464 extra stator harmonic currents reduction.

## APPENDIX A

## VOLTAGE VECTORS APPLYING TIMES CALCULATION

The inverter output voltage vectors are represented in Figs. 3, 467  
and Fig. 5 by decimal number  $k$  equivalent to the binary number 468  
formed by the instantaneous values of the switching functions 469  
defined as: 470

$$k = K_{a1} \times 2^0 + K_{b1} \times 2^1 + K_{c1} \times 2^2 + K_{a2} \times 2^3 + K_{b2} \times 2^4 + K_{c2} \times 2^5. \quad (A1)$$

The instantaneous values of the six-phase VSI output voltage 471  
vectors  $(v_{a1}, v_{b1}, v_{c1}, v_{a2}, v_{b2}, v_{c2})$  can be determined by using 472  
the inverter connection matrix  $[Mc]$  as follows: 473

$$[v_{a1} \ v_{b1} \ v_{c1} \ v_{a2} \ v_{b2} \ v_{c2}]^T = [Mc][K_{a1} \ K_{b1} \ K_{c1} \ K_{a2} \ K_{b2} \ K_{c2}]^T \quad (A2)$$

where

$$[Mc] = \frac{V_{dc}}{3} \begin{bmatrix} 2 & -1 & -1 & 0 & 0 & 0 \\ -1 & 2 & -1 & 0 & 0 & 0 \\ -1 & -1 & 2 & 0 & 0 & 0 \\ 0 & 0 & 0 & 2 & -1 & -1 \\ 0 & 0 & 0 & -1 & 2 & -1 \\ 0 & 0 & 0 & -1 & -1 & 2 \end{bmatrix}. \quad (A3)$$

The inverter output voltage vectors are transformed into 475  
 $(\alpha-\beta)$ ,  $(x-y)$ , and  $(o_1-o_2)$  planes by means of the transfor- 476  
mation matrix  $[Ts]^{-1}$  given in (1), as: 477

$$[v_{s\alpha k} \ v_{s\beta k} \ v_{sxk} \ v_{syk} \ v_{o1k} \ v_{o2k}]^T = [Ts]^{-1}[v_{a1} \ v_{b1} \ v_{c1} \ v_{a2} \ v_{b2} \ v_{c2}]^T \quad (A4)$$

For example, when the reference voltage vector is located in sector 1, voltage vectors 41, 9, 11, and 15 are selected and their equivalent binary numbers are defined as:

$$\begin{aligned} 41 &= [1 \ 0 \ 1|0 \ 0 \ 1] \\ 9 &= [0 \ 0 \ 1|0 \ 0 \ 1] \\ 11 &= [0 \ 0 \ 1|0 \ 1 \ 1] \\ 15 &= [0 \ 0 \ 1|1 \ 1 \ 1]. \end{aligned} \quad (A5)$$

Then the  $(\alpha-\beta)$ , and  $(x-y)$  voltages can be calculated by using (A2), and (A4), as follows:

$$\begin{aligned} &\begin{bmatrix} V_{s\alpha 41} & V_{s\alpha 9} & V_{s\alpha 11} & V_{s\alpha 15} \\ V_{s\beta 41} & V_{s\beta 9} & V_{s\beta 11} & V_{s\beta 15} \\ V_{sx 41} & V_{sx 9} & V_{sx 11} & V_{sx 15} \\ V_{sy 41} & V_{sy 9} & V_{sy 11} & V_{sy 15} \end{bmatrix} \\ &= \frac{V_{dc}}{2\sqrt{3}} \begin{bmatrix} 2+\sqrt{3} & 2+\sqrt{3} & 1+\sqrt{3} & \sqrt{3} \\ -1 & 1 & 1+\sqrt{3} & 1 \\ 2-\sqrt{3} & 2-\sqrt{3} & 1-\sqrt{3} & -\sqrt{3} \\ -1 & 1 & 1-\sqrt{3} & 1 \end{bmatrix}. \end{aligned} \quad (A6)$$

The voltage vectors applying times:  $t_1$ ,  $t_2$ ,  $t_3$  and  $t_4$  are obtained as:

$$\begin{aligned} \begin{bmatrix} t_1 \\ t_2 \\ t_3 \\ t_4 \end{bmatrix} &= \begin{bmatrix} V_{s\alpha 41} & V_{s\alpha 9} & V_{s\alpha 11} & V_{s\alpha 15} \\ V_{s\beta 41} & V_{s\beta 9} & V_{s\beta 11} & V_{s\beta 15} \\ V_{sx 41} & V_{sx 9} & V_{sx 11} & V_{sx 15} \\ V_{sy 41} & V_{sy 9} & V_{sy 11} & V_{sy 15} \end{bmatrix}^{-1} \begin{bmatrix} v_{s\alpha}^* T_s \\ v_{s\beta}^* T_s \\ v_{sx}^* T_s \\ v_{sy}^* T_s \end{bmatrix} \\ t_0 &= T_s - (t_1 + t_2 + t_3 + t_4). \end{aligned} \quad (A7)$$

Substituting (A6) in (A7), the applying times can be calculated as follows:

$$\begin{aligned} \begin{bmatrix} t_1 \\ t_2 \\ t_3 \\ t_4 \end{bmatrix} &= \frac{T_s}{2V_{dc}} \begin{bmatrix} 1 & -\sqrt{3} & -1 & -\sqrt{3} \\ \sqrt{3}-1 & \sqrt{3}-1 & \sqrt{3}+1 & \sqrt{3}+1 \\ 0 & 2 & 0 & v-2 \\ -(\sqrt{3}-2) & -1 & -(\sqrt{3}+2) & 1 \end{bmatrix} \begin{bmatrix} v_{s\alpha}^* \\ v_{s\beta}^* \\ v_{sx}^* \\ v_{sy}^* \end{bmatrix}. \end{aligned} \quad (A8)$$

With  $v_{sx}^* = v_{sy}^* = 0$ , (A8) can be written as:

$$\begin{aligned} \begin{bmatrix} t_1 \\ t_2 \\ t_3 \\ t_4 \end{bmatrix} &= \frac{T_s}{2V_{dc}} \begin{bmatrix} 1 & -\sqrt{3} \\ \sqrt{3}-1 & \sqrt{3}-1 \\ 0 & 2 \\ -(\sqrt{3}-2) & -1 \end{bmatrix} \begin{bmatrix} v_{s\alpha}^* \\ v_{s\beta}^* \end{bmatrix} = \begin{bmatrix} T_2 \\ T_5 \\ T_4 \\ -T_1 \end{bmatrix}. \end{aligned} \quad (A9)$$

## APPENDIX B

### MAXIMUM MODULATION INDEX CALCULATION

The maximum modulation index  $m_{\max}$  can be obtained by solving  $t_0 = T_s - (t_1 + t_2 + t_3 + t_4) = 0$ . For example in sector 1, the sum of the applying times of the active voltage vectors is calculated from (A9) as:

$$\theta \in \left[0, \frac{\pi}{12}\right] \quad t_1 + t_2 + t_3 + t_4 = \frac{T_s}{V_{dc}} v_{s\alpha}^* \quad (B1)$$

where  $v_{s\alpha}^* = \sqrt{3}V_{1m} \cos(\theta)$ ,  $v_{s\beta}^* = \sqrt{3}V_{1m} \sin(\theta)$

$$V_{1m} = mV_{1m6step} = m2V_{dc}/\pi.$$

When

$$t_0 = 0 : T_s = t_1 + t_2 + t_3 + t_4 = 2\sqrt{3}\frac{T_s}{\pi}m \cos(\theta) \quad (B2)$$

From (B2), the modulation index equation can be given as:

$$m = \frac{\pi}{2\sqrt{3} \cos(\theta)}. \quad (B3)$$

To determine the angle  $\theta$  corresponding to  $m_{\max}$ , (B3) is derived:

$$\frac{dm}{d\theta} = \frac{\pi \sin(\theta)}{2\sqrt{3} \cos^2(\theta)}. \quad (B4)$$

Equation (B4) is solved for  $\theta = 0$ . Thus, replacing  $\theta$  in (B3):

$$m_{\max} = \frac{\pi}{2\sqrt{3} \cos(0)} = \frac{\pi}{2\sqrt{3}} \approx 0.907. \quad (B5)$$

## APPENDIX C

### ANALYTICAL FORMULAS OF THE RMS HARMONIC FLUX

The per-fundamental cycle rms normalized harmonic flux  $\tilde{\lambda}_{sfrms}$  was calculated for all the discussed PWM techniques. Only the analytical formulas of the proposed 24-sector PWMs are presented here and the ones of the 12-sector PWMs can be found in [10]. These formulas are given below.

#### A. Continuous Modulation C6 $\phi$ SVPWM24

$$\begin{aligned} \tilde{\lambda}_{s\alpha\beta frms}^2(m) &= \frac{1}{48}m^2 + \frac{1}{144\pi^2} \\ &\times (56\sqrt{3} + 63\sqrt{6} - 57\sqrt{2} - 228)m^3 \\ &+ \frac{1}{32\pi^3}(24\pi + 27 - 21\sqrt{3} - 8\sqrt{3}\pi)m^4 \\ \tilde{\lambda}_{sxy frms}^2(m) &= \frac{1}{144\pi^2}(63\sqrt{6} + 18 - 52\sqrt{3} - 57\sqrt{2})m^3. \end{aligned} \quad (C1)$$

#### B. Discontinuous Modulation D6 $\phi$ SVPWM24-B1

$$\begin{aligned} \tilde{\lambda}_{s\alpha\beta frms}^2(m) &= \frac{25}{432}m^2 - \frac{25}{5184\pi^2} \\ &\times (633\sqrt{2} + 408 - 56\sqrt{3} - 387\sqrt{6})m^3 \\ &- \frac{25}{576\pi^3}(15\sqrt{3} + 8\sqrt{3}\pi - 24\pi - 45)m^4 \\ \tilde{\lambda}_{sxy frms}^2(m) &= \frac{25}{5184\pi^2}(63\sqrt{6} + 18 - 52\sqrt{3} - 57\sqrt{2})m^3. \end{aligned} \quad (C2)$$

#### C. Discontinuous Modulation D6 $\phi$ SVPWM24-B2

$$\begin{aligned} \tilde{\lambda}_{s\alpha\beta frms}^2(m) &= \frac{1}{27}m^2 - \frac{1}{324\pi^2} \\ &\times (129\sqrt{2} + 45\sqrt{6} + 48 - 56\sqrt{3})m^3 \\ &+ \frac{1}{6\pi^3}(2\pi + 3 - \sqrt{3})m^4 \\ \tilde{\lambda}_{sxy frms}^2(m) &= \frac{1}{324\pi^2}(63\sqrt{6} + 18 - 52\sqrt{3} - 57\sqrt{2})m^3. \end{aligned} \quad (C3)$$

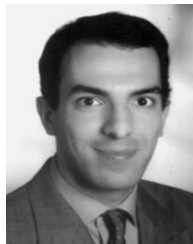
## REFERENCES

- 510
- 511 [1] V. T. Somasekhar, K. Gopakumar, M. R. Baiju, K. K. Mohapatra, and  
512 L. Umanand, "A multilevel inverter system for an induction motor with  
513 open-end windings," *IEEE Trans. Ind. Electron.*, vol. 52, no. 3, pp. 824–  
514 836, Jun. 2005.
- 515 [2] R. C. Portillo *et al.*, "Modeling strategy for back-to-back three-level con-  
516 verters applied to high-power wind turbines," *IEEE Trans. Ind. Electron.*,  
517 vol. 53, no. 5, pp. 1483–1491, Oct. 2006.
- 518 [3] A. K. Gupta and A. M. Khambadkone, "A space vector PWM scheme for  
519 multilevel inverters based on two-level space vector PWM," *IEEE Trans.*  
520 *Ind. Electron.*, vol. 53, no. 5, pp. 1631–1639, Oct. 2006.
- 521 [4] K. Hatua and V. T. Ranganathan, "Direct torque control schemes for  
522 split-phase induction machine," *IEEE Trans. Ind. Appl.*, vol. 41, no. 5,  
523 pp. 1243–1254, Sep./Oct. 2005.
- 524 [5] Y. Zhao and T. A. Lipo, "Space vector PWM control of dual three-phase  
525 induction machine using vector space decomposition," *IEEE Trans. Ind.*  
526 *Appl.*, vol. 31, no. 5, pp. 1100–1109, Sep./Oct. 1995.
- 527 [6] M. A. Abbas, R. Christen, and T. M. Jahns, "Six-phase voltage source  
528 inverter driven induction motor," *IEEE Trans. Ind. Appl.*, vol. 1A-20, no. 5,  
529 pp. 1251–1259, Sep./Oct. 1984.
- 530 [7] D. Hadiouche, H. Razik, and A. Rezzoug, "On the modeling and design  
531 of dual-stator windings to minimize circulating harmonic currents for VSI  
532 fed AC machines," *IEEE Trans. Ind. Appl.*, vol. 40, no. 2, pp. 506–515,  
533 Mar./Apr. 2004.
- 534 [8] A. R. Muñoz and T. A. Lipo, "Dual stator winding induction machine  
535 drive," *IEEE Trans. Ind. Appl.*, vol. 36, no. 5, pp. 1369–1379,  
536 Sep./Oct. 2000.
- 537 [9] K. Gopakumar, V. T. Ranganathan, and S. R. Bhat, "Split-phase induction  
538 motor operation from PWM voltage source inverter," *IEEE Trans. Ind.*  
539 *Appl.*, vol. 29, no. 5, pp. 927–932, Sep./Oct. 1993.
- 540 [10] D. Hadiouche, L. Baghli, and A. Rezzoug, "Space vector PWM  
541 techniques for dual three-phase AC machine: Analysis, performance  
542 evaluation, and DSP implementation," *IEEE Trans. Ind. Appl.*, vol. 42,  
543 no. 4, pp. 1112–1122, Jul./Aug. 2006.
- 544 [11] R. Bojoi, M. Lazzari, F. Profumo, and A. Tenconi, "Digital field-oriented  
545 control for dual three-phase induction motor drives," *IEEE Trans. Ind.*  
546 *Appl.*, vol. 39, no. 3, pp. 752–760, May/Jun. 2003.
- 547 [12] K. K. Mohapatra, R. S. Kanchan, M. R. Baiju, P. N. Tekwani, and  
548 K. Gopakumar, "Independent field-oriented control of two split-phase  
549 induction motors from a single six-phase inverter," *IEEE Trans. Ind.*  
550 *Electron.*, vol. 52, no. 5, pp. 1372–1382, Oct. 2005.
- 551 [13] W. Tiejun, G. Chenglin, C. Yongbing, and J. Xiaoyi, "Research on har-  
552 monics of multiphase induction motors," in *Proc. IEEE IEMDC*, Antalya,  
553 Turkey, May 3–5, 2007, vol. 2, pp. 1524–1528.
- 554 [14] J. W. Kolar, H. Ertl, and F. C. Zach, "Influence of the modulation method  
555 on the conduction and switching losses of a PWM converter system,"  
556 *IEEE Trans. Ind. Appl.*, vol. 27, no. 6, pp. 1063–1075, Nov./Dec. 1991.
- 557 [15] K. Marouani, L. Baghli, D. Hadiouche, A. Kheloui, and A. Rezzoug,  
558 "Discontinuous SVPWM techniques for double star induction motor  
559 drive control," in *Proc. IEEE IECON*, Paris, France, Nov. 6–10, 2006,  
560 pp. 902–907.
- 561 [16] G. K. Singh, K. Nam, and S. K. Lim, "A simple indirect field-oriented  
562 control scheme for multiphase induction machine," *IEEE Trans. Ind.*  
563 *Electron.*, vol. 52, no. 4, pp. 1177–1184, Aug. 2005.
- 564 [17] D. C. Lee and G. M. Lee, "Linear control of inverter output voltage in  
565 overmodulation," *IEEE Trans. Ind. Electron.*, vol. 44, no. 4, pp. 590–592,  
566 Aug. 1997.
- 567 [18] S. R. Bowes and Y. S. Lai, "The relationship between space-vector mod-  
568 ulation and regular-sampled PWM," *IEEE Trans. Ind. Electron.*, vol. 44,  
569 no. 5, pp. 670–679, Oct. 1997.
- 570 [19] O. Ojo, "The generalized discontinuous PWM scheme for three-phase  
571 voltage source inverters," *IEEE Trans. Ind. Electron.*, vol. 51, no. 6,  
572 pp. 1280–1289, Dec. 2004.
- 573 [20] A. M. Hava, R. J. Kerkman, and T. A. Lipo, "Simple analytical and graph-  
574 ical methods for carrier-based PWM-VSI drives," *IEEE Trans. Power*  
575 *Electron.*, vol. 14, no. 1, pp. 49–61, Jan. 1999.
- 576 [21] S. Ogasawara, H. Akagi, and A. Nabae, "A novel PWM scheme of voltage  
577 source inverters based on space vector theory," in *Proc. EPE*, Aachen,  
578 Germany, Oct. 1989, pp. 1197–1202.
- 579 [22] H. W. van der Broeck, H. C. Skudelny, and G. V. Stanke, "Analysis and  
580 realization of a pulsewidth modulator based on voltage space vectors,"  
581 *IEEE Trans. Ind. Appl.*, vol. 24, no. 1, pp. 142–150, Jan./Feb. 1988.
- 582 [23] J. Holtz and B. Beyer, "Optimal pulse width modulation for AC servos  
583 and low-cost industrial drives," *IEEE Trans. Ind. Appl.*, vol. 30, no. 4,  
584 pp. 1039–1047, Jul./Aug. 1994.
- 585 [24] *TMS320F/C240 DSP Controllers Reference Guide, Peripheral and Spe-*  
586 *cific Devices*, Texas Instruments, Dallas, TX, 1999. Literature Number  
587 SPRU161C.



**Khoudir Marouani** was born in 1972. He received the Degree of Engineer in automatics and the Degree of Magister in electrical engineering from the Poly-technic Military School (EMP), Algiers, Algeria, in 1996 and 2000, respectively, where he is currently working toward the Ph.D. degree in the Electrical Engineering Laboratory.

He is currently working as a Research and Teaching Assistant with the Electrical Engineering Laboratory, EMP. His research interests include power electronics, electrical drives and active power filters.



**Lotfi Baghli** was born in 1971. He received the Electrical Engineering Diploma degree (with honors) from the Ecole Nationale Polytechnique, Algiers, Algeria, in 1989, and the DEA degree in electrical engineering from the Université Henri Poincaré, Nancy, France, in 1995 and 1999, respectively.

He is currently a Lecturer at IUFM de Lorraine and a member of Groupe de Recherche en Electrotechnique et Electronique de Nancy, Nancy. His works concern digital control using DSP, PSO and genetic algorithms applied to the control and identification of electrical machines.



**Djafar Hadiouche** was born in 1974. He received the Ph.D. degree in electrical engineering from the University Henri Poincaré, Nancy, France, in 2001.

Until 2002, he was Assistant Lecturer in the same university and did research in the laboratory of the "Groupe de Recherche en Electrotechnique et Electronique de Nancy," Nancy. Since 2003, he has been a Motion Specialist Engineer with GE Fanuc Automation Solutions Europe, Echternach, Luxembourg. His main tasks include servosizing, tools and motion programs development, electronic cam profiling and motion technical training. His main research interests concern multiphase ac machines, their modeling, identification, pulsewidth modulation techniques, and vector control.

Dr. Hadiouche received the Best Prize Paper Award from the Electric Machine Committee at the 2001 IEEE IAS Annual Meeting.



**Abdelaziz Kheloui** was born in 1969. He received the M.Sc.Eng. degree from the Ecole Nationale d'ingénieurs et Techniciens d'Algérie, Algiers, Algeria, in 1990, and the Ph.D. degree in electrical engineering from the Institut National Polytechnique de Lorraine, Nancy, France, in 1994.

Since 1994, he has been a Researcher and a Teacher at the electrical engineering laboratory of the Polytechnic Military School, Algiers, Algeria. His current research interests are control of electrical drives and power electronics.



**Abderrezak Rezzoug** was born in 1948. He received the Electrical Engineer degree, Dr. Ing. diploma, and Ph.D. degree from ENSEM Institut National Polytechnique de Lorraine, Nancy, France, in 1972, 1979, and 1987, respectively.

He is currently a Professor in electrical engineering at the Université Henri Poincaré, Nancy. As a member of the Groupe de Recherche en Electrotechnique et Electronique de Nancy, Nancy, his main areas of research concern electrical machines, their identification, diagnostic and control, and superconducting applications.



## AUTHOR QUERIES

AUTHOR PLEASE ANSWER ALL QUERIES

AQ1 = “1972” was assumed as the author’s birth year. Please check if appropriate.

AQ2 = “1971” was assumed as the author’s birth year. Please check if appropriate.

AQ3 = Please provide the expanded form of the acronym “IUFM”.

AQ4 = “1974” was assumed as the author’s birth year. Please check if appropriate.

AQ5 = “1969” was assumed as the author’s birth year. Please check if appropriate.

AQ6 = “1948” was assumed as the author’s birth year. Please check if appropriate.

AQ7 = Please provide the expanded form of the acronym “ENSEM”.

Note: Figure citations were renumbered. The original sequence was 1-2-3-4-5-6-7-9-8.

END OF ALL QUERIES

# A New PWM Strategy Based on a 24-Sector Vector Space Decomposition for a Six-Phase VSI-Fed Dual Stator Induction Motor

Khoudir Marouani, Lotfi Baghli, Djafar Hadiouche, Abdelaziz Kheloui, and Abderrezak Rezzoug

**Abstract**—This paper presents a new space vector pulsewidth modulation (SVPWM) technique for the control of six-phase voltage source inverter (VSI)-fed dual stator induction machines (DSIM). A DSIM is an induction machine which has two sets of three-phase stator windings spatially shifted by 30 electrical degrees and fed by two three-phase VSIs. Despite their advantage of power segmentation, these machines are characterized by large zero sequence harmonic currents, and in particular those of order  $6k \pm 1$ , which are due to the mutual cancellation between the two stator windings. The proposed SVPWM scheme, while easy to implement digitally, reduces significantly these extra stator harmonic currents. Experimental results, collected from a 15 kW prototype machine controlled by a digital signal processor are presented and discussed.

**Index Terms**—Dual stator induction machines (DSIM), six-phase voltage source inverter (VSI), space vector pulsewidth modulation (SVPWM).

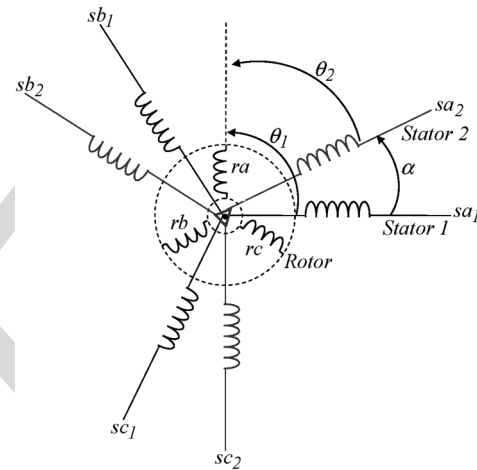


Fig. 1. DSIM windings.

## I. INTRODUCTION

NOWADAYS, electrical machine drives are widely used in industrial applications and transportation systems such as electric/hybrid vehicles, traction locomotives and electric propulsion ships, where high-power levels in conjunction with high-performance requirements are more and more demanded. To achieve these high ratings, there are two possible approaches; one focuses on the converter side by increasing the number of output voltage levels and the other one on the machine side by increasing the number of phases. In the first approach, the idea is to divide the high dc bus voltage into multiple low levels and therefore to distribute the high power required among cells of reduced-voltage power switches without the problem of dynamic voltage sharing encountered in the series connection of active devices. However, increasing the number of inverter levels adds to the control complexity and may introduce some voltage imbalance problems [1]–[3]. It is a solution well suited for high-power and high-voltage utility ap-

plications. For adjustable speed drives, however, an alternative approach is to use a multiphase machine, i.e., a machine with more than three phases in the stator, since the number of phases is not imposed anyway, given that the machine is connected to the electric supply through a dc/ac converter. The number of phases could be used instead as an additional degree of freedom in the overall system design [4].

Although the answer to the question whether it is better to use a multilevel inverter-fed three-phase machine or a multiphase machine depends on the application, it is undeniable that the latter option offers several advantages which may make it appear very attractive. In fact, the most significant features are a low torque ripple, a reduction in the power per phase and fault-tolerance capability. Other interesting advantages can be pointed out, such as a better torque production per ampere for the same machine volume, higher efficiency and improved reliability [5], [6].

A common type of multiphase machine is the dual stator induction machine (DSIM), where two sets of three-phase windings, spatially phase shifted by 30 electrical degrees, share a common stator magnetic core as shown in Fig. 1.

Due to the development of fast switching power semiconductor devices, voltage source inverters (VSIs) are preferred in variable speed machine drives. As VSI-fed multiphase machines are gaining increasing interest for high-power applications, various pulsewidth modulation (PWM) techniques have been developed accordingly, as they strongly affect the overall inverter efficiency and output voltage waveform quality.

Manuscript received February 28, 2007; revised September 24, 2007.

K. Marouani and A. Kheloui are with the Electrical Engineering Laboratory, Polytechnic Military School, 16111 Algiers, Algeria (e-mail: marouani\_khoudir@yahoo.fr; akheloui@caramail.com).

L. Baghli and A. Rezzoug are with the Groupe de Recherche en Electrotechnique et Electronique de Nancy, CNRS UMR 7037, Université Henri Poincaré, 54506 Nancy Cedex, France (e-mail: lotfi.baghli@green.uhp-nancy.fr; abderrezak.rezzoug@green.uhp-nancy.fr).

D. Hadiouche is with the GE Fanuc Automation Solutions Europe, 6468 Echternach, Luxembourg (e-mail: djafar.hadiouche@wanadoo.fr).

Color versions of one or more of the figures in this paper are available online at <http://ieeexplore.ieee.org>.

Digital Object Identifier 10.1109/TIE.2008.918486

In a VSI-fed DSIM, the two stator windings are mutually coupled and small unbalances in the two supply voltages may generate high currents [7]. Furthermore, because of the low impedance seen by the voltage harmonic components generated by the switched voltage waveforms, harmonic currents of high level are circulating uselessly in the two stator windings, adding to the overall losses and therefore to the semiconductor devices ratings [8], [9].

To minimize these extra harmonic currents in a six-phase VSI-fed DSIM, a new 24-sector PWM technique is proposed in this paper and tested on a 15 kW laboratory machine. The digital implementation is carried out on a DS1104 dSPACE controller board. A comparative study between the proposed technique and similar space vector PWM (SVPWM) techniques [5], [10], based on analytical harmonic current analysis, is also developed and discussed.

## II. MACHINE MODEL

The machine model is based on the assumption that space harmonics and magnetic saturation are negligible, and that the two stator three-phase windings are identical and symmetrical with the two neutrals being isolated. In order to derive a practical model suitable for control, a decoupling transformation matrix is used, as proposed in [5]–[7]. The matrix has the following form:

$$[T_s]^{-1} = \frac{1}{\sqrt{3}} \begin{bmatrix} 1 & -\frac{1}{2} & -\frac{1}{2} & \frac{\sqrt{3}}{2} & -\frac{\sqrt{3}}{2} & 0 \\ 0 & \frac{\sqrt{3}}{2} & -\frac{\sqrt{3}}{2} & \frac{1}{2} & \frac{1}{2} & -1 \\ 1 & -\frac{1}{2} & -\frac{1}{2} & -\frac{\sqrt{3}}{2} & \frac{\sqrt{3}}{2} & 0 \\ 0 & -\frac{\sqrt{3}}{2} & \frac{\sqrt{3}}{2} & \frac{1}{2} & \frac{1}{2} & -1 \\ 1 & 1 & 1 & 0 & 0 & 0 \\ 0 & 0 & 0 & 1 & 1 & 1 \end{bmatrix}. \quad (1)$$

By applying (1) to the voltage vector equations, the overall machine model is transformed into three decoupled submodels, written in three independent space coordinates, identified as  $(\alpha-\beta)$ ,  $(x-y)$ , and  $(o_1-o_2)$ , respectively.

The machine voltage submodel in  $(\alpha-\beta)$  coordinates can be written as:

$$\begin{bmatrix} v_{s\alpha} \\ v_{s\beta} \\ v_{r\alpha} \\ v_{r\beta} \end{bmatrix} = \begin{bmatrix} R_s & 0 & 0 & 0 \\ 0 & R_s & 0 & 0 \\ 0 & M\dot{\theta} & R_r & L_r\dot{\theta} \\ -M\dot{\theta} & 0 & -L_r\dot{\theta} & R_r \end{bmatrix} \begin{bmatrix} i_{s\alpha} \\ i_{s\beta} \\ i_{r\alpha} \\ i_{r\beta} \end{bmatrix} + \begin{bmatrix} L_s & 0 & M & 0 \\ 0 & L_s & 0 & M \\ M & 0 & L_r & 0 \\ 0 & M & 0 & L_r \end{bmatrix} \frac{d}{dt} \begin{bmatrix} i_{s\alpha} \\ i_{s\beta} \\ i_{r\alpha} \\ i_{r\beta} \end{bmatrix} \quad (2)$$

where  $\dot{\theta} = \Omega_m$  is the rotor mechanical speed, and  $L_s = L_{ls} + 3L_{ms}$ ,  $L_r = L_{lr} + (3/2)L_{mr}$ ,  $M = (3/\sqrt{2})M_{sr}$ .  $L_{ls}$  and  $L_{lr}$  are the stator and rotor leakage inductances in  $(\alpha-\beta)$  coordinates, respectively.

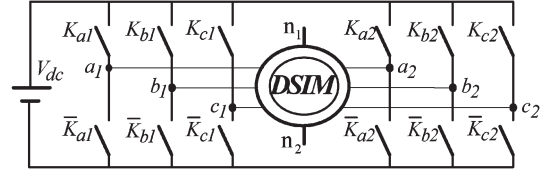


Fig. 2. Six-phase VSI fed DSIM.

The DSIM  $(\alpha-\beta)$  submodel expressed in the stationary reference frame is similar to the three-phase induction machine model [11].

The machine voltage submodel in  $(x-y)$  coordinates is given by:

$$\begin{bmatrix} v_{sx} \\ v_{sy} \end{bmatrix} = \begin{bmatrix} R_s & 0 \\ 0 & R_s \end{bmatrix} \begin{bmatrix} i_{sx} \\ i_{sy} \end{bmatrix} + \begin{bmatrix} L_{lsxy} & 0 \\ 0 & L_{lsxy} \end{bmatrix} \frac{d}{dt} \begin{bmatrix} i_{sx} \\ i_{sy} \end{bmatrix} \quad (3)$$

where  $L_{lsxy}$  is the transformed stator leakage inductance in  $(x-y)$  coordinates.

The machine voltage submodel in  $(o_1-o_2)$  coordinates is expressed as follows:

$$\begin{bmatrix} v_{so1} \\ v_{so2} \\ v_{ro} \end{bmatrix} = \begin{bmatrix} R_s & 0 & 0 \\ 0 & R_s & 0 \\ 0 & 0 & R_r \end{bmatrix} \begin{bmatrix} i_{so1} \\ i_{so2} \\ i_{ro} \end{bmatrix} + \begin{bmatrix} L_{lso} & 0 & 0 \\ 0 & L_{lso} & 0 \\ 0 & 0 & L_{lr} \end{bmatrix} \frac{d}{dt} \begin{bmatrix} i_{so1} \\ i_{so2} \\ i_{ro} \end{bmatrix} \quad (4)$$

where  $L_{lso}$  is the transformed stator leakage inductance in  $(o_1-o_2)$  coordinates.

The electromagnetic torque of the DSIM is expressed only in terms of stator and rotor  $(\alpha-\beta)$  current components, since the  $(x-y)$  and  $(o_1-o_2)$  counterparts do not contribute to the electromechanical energy conversion, as shown by (3) and (4). The expression of the electromagnetic torque is then as follows:

$$T_e = pM(i_{s\beta}i_{r\alpha} - i_{s\alpha}i_{r\beta}) \quad (5)$$

where  $p$  is the number of pole pairs.

## General Remarks

The  $(x-y)$  and  $(o_1-o_2)$  current components do not contribute to the air-gap flux linkages. Hence, they are limited only by the stator resistance and leakage inductance [12], [13]. They produce only losses and therefore must be kept equal to zero or as small as possible.

The transformed voltage equations in the three subframes are well decoupled and, as a result, both machine analysis and control are greatly simplified.

## III. SVPWM CONTROL OF A DOUBLE-STAR INDUCTION MOTOR

The drive system is a six-phase VSI fed DSIM, as shown in Fig. 2. A combinatorial analysis of the inverter switch states shows 64 switching modes. Thus, 64 different voltage vectors can be applied to the machine. Each voltage vector is represented by a decimal number corresponding to the binary number  $(K_{c2}K_{b2}K_{a2}K_{c1}K_{b1}K_{a1})$ , which gives the state of

the upper switches. By using the  $(6 \times 6)$  transformation matrix  $[\mathbf{T}_s]^{-1}$ , each voltage vector can be decomposed into  $(\alpha-\beta)$ ,  $(x-y)$ , and  $(o_1-o_2)$  voltages. The  $(o_1-o_2)$  ones are all equal to zero because the neutrals ( $n_1, n_2$ ) of the two winding sets are isolated. So the SVPWM strategy operates in two complex planes  $(\alpha-\beta)$  and  $(x-y)$ . Four variables need to be controlled simultaneously during each sampling period, by generating maximum  $(\alpha-\beta)$  and minimum  $(x-y)$  voltage amplitudes. Therefore, during each sampling period, a set of four active voltage vectors must be chosen to fulfil these two conditions, according to the reference voltage vector location. There are numerous ways for choosing such a set.

#### A. Six-Phase SVPWM Techniques

The principle of the PWM control techniques proposed in [5] and [10] is to choose switching sequences in such a way that two consecutive nonzero voltage vectors are practically opposite in phase in the  $(x-y)$  plane. In this way, each change in the applied vectors leads to a sequence of increases and decreases in  $(x-y)$  currents around zero. Moreover, in order to minimize  $(x-y)$  harmonic currents and maintain the lowest switching frequency, there are different choices to allocate zero voltage vectors (0, 7, 56 or 63) within the switching sequences. Thus, the switching sequences presented in [10] lead to continuous and discontinuous modulation techniques and, consequently, to different harmonic distortion characteristics. A modulation technique is continuous when on/off switching occurs within every sampling period, for all inverter legs and all sectors. A modulation technique is discontinuous when one (or more) inverter leg stops switching, i.e., the corresponding phase voltage is clamped to the positive or negative dc bus for at least one sector [14].

#### B. 12-Sector SVPWM Technique

In the SVPWM technique addressed in [5], only the  $(\alpha-\beta)$  voltage vectors having maximum magnitude (45, 41, 9, 11, 27, 26, 18, 22, 54, 52, 36, 37) are employed to synthesize the reference voltage vector  $v_{s\alpha\beta}^*$ . These voltage vectors divide the  $(\alpha-\beta)$  plane into 12 sectors and each sector is  $\pi/6$  rad, as shown in Fig. 3. For example, voltage vectors 45, 41, 9, 11 and 1 are selected when the reference voltage vector is located in sector 1. As shown in Fig. 4, continuous and discontinuous modulation techniques can be obtained according to the switching sequences given below.

1) *Continuous Modulation C6  $\phi$  SVPWM12*: For example, when the reference voltage vector is located in sector 1, a continuous modulation technique (C6  $\phi$  SVPWM12) is obtained with the following sequence:

$$[7-45-41-56-9-11-7|7-11-9-56-41-45-7].$$

2) *Discontinuous Modulation D6  $\phi$  SVPWM12-A*: For the same sector 1, a discontinuous modulation technique (D6  $\phi$  SVPWM12-A) can be obtained with the following sequence:

$$[7-45-41-9-11-7|7-11-9-41-45-7].$$

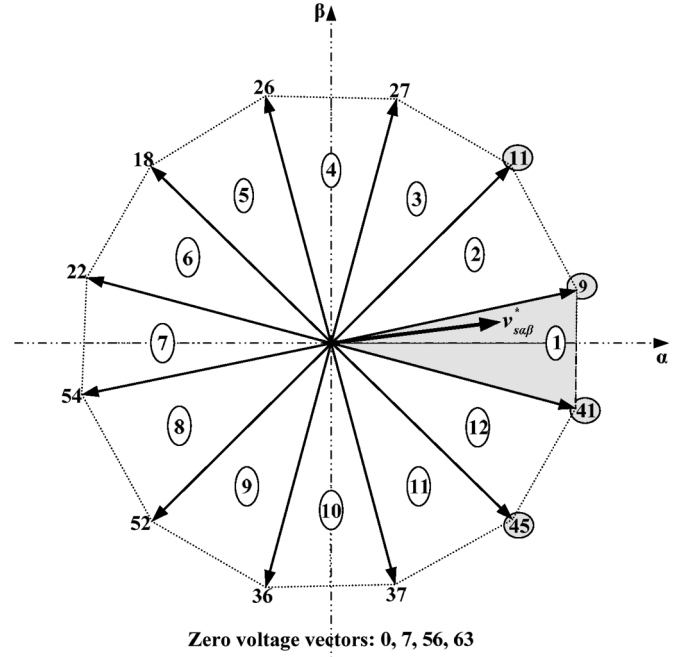


Fig. 3. Presentation of the inverter voltage vectors having maximum magnitude in  $(\alpha-\beta)$  plane.

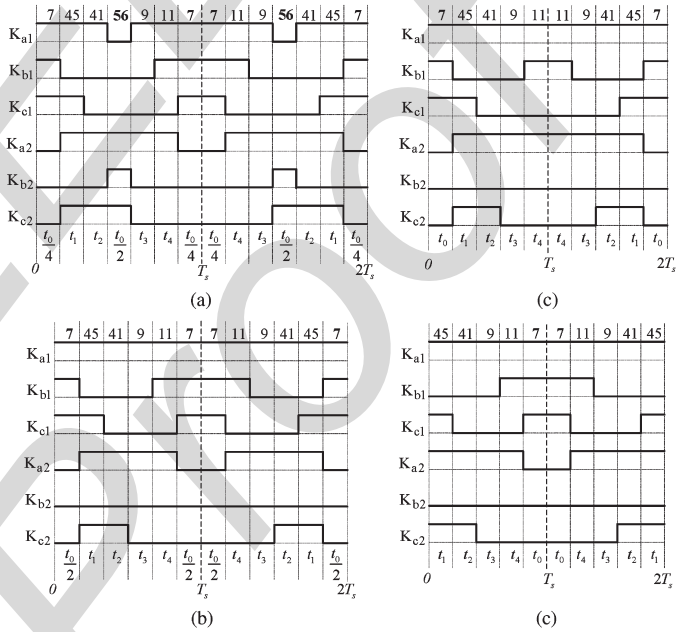


Fig. 4. Twelve-sector SVPWM switching sequences when the reference voltage vector is located in sector 1. (a) C6  $\phi$  SVPWM12. (b) D6  $\phi$  SVPWM12-A. (c) D6  $\phi$  SVPWM12-B1. (d) D6  $\phi$  SVPWM12-B2.

3) *Discontinuous Modulation D6  $\phi$  SVPWM12-B1*: In the D6  $\phi$  SVPWM12-B1, the zero-voltage vectors are applied at the beginning and at the end of the switching sequence as follows:

$$[7-45-41-9-11|11-9-41-45-7].$$

4) *Discontinuous Modulation D6  $\phi$  SVPWM12-B2*: In the D6  $\phi$  SVPWM12-B2, the zero-voltage vectors are applied in the middle of the switching sequence as follows:

$$[45-41-9-11-7|7-11-9-41-45].$$



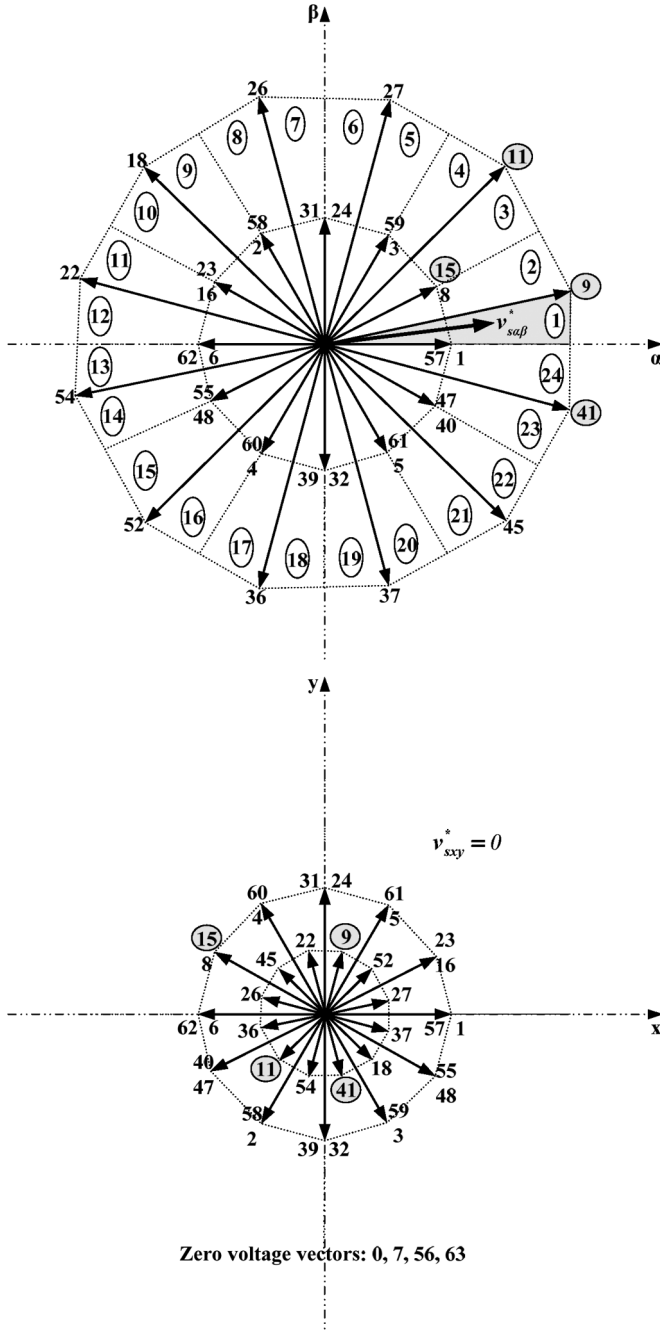


Fig. 5. Presentation of the inverter voltage vectors having maximum and half magnitude in  $(\alpha-\beta)$ , and  $(x-y)$  planes.

### 191 C. Proposed 24-Sector SVPWM Technique

192 As shown in Fig. 4, the switching pattern corresponding  
193 to the switching sequences of the 12-sector PWM techniques  
194 presents asymmetrical waveforms and usually more than two  
195 transitions (from low to high or from high to low) occur on  
196 the corresponding PWM outputs within a sampling period,  
197 which increases the switching frequency of the inverter legs  
198 and causes difficulties for digital signal processor (DSP) im-  
199 plementation of these strategies. Accordingly, some additional  
200 adaptations in DSP programs are necessary to ensure successful  
201 experiments [15], [16].

202 To overcome these drawbacks, the new 24-sector SVPWM  
203 technique proposed in this paper combines the maximum

magnitude  $(\alpha-\beta)$  voltage vectors and the ones with half  
204 magnitude (1, 57, 8, 15, 3, 59, 24, 31, 2, 58, 16, 23, 6, 205  
62, 48, 55, 4, 60, 32, 39, 5, 61, 40, 47) generated by one  
206 inverter. These voltage vectors divide the  $(\alpha-\beta)$  plane into  
207 twenty four  $\pi/12$ -rad sectors, as shown in Fig. 5. In each  
208 sampling period, the reference voltage vector is achieved by  
209 selecting a set of three voltage vectors among those having  
210 maximum magnitude and a fourth vector among the ones with  
211 half magnitude. For example, voltage vectors 41, 9, 11 and 15  
212 are selected when the reference voltage vector is located in  
213 sector 1. Then, the voltage vectors applying times:  $t_1, t_2, t_3$  and  
214  $t_4$  are obtained as explained in Appendix A. For the remaining  
215 time  $t_0 = T_s - (t_1 + t_2 + t_3 + t_4)$ , zero state vectors (0, 7, 56  
216 or 63) are applied. Consequently, simple PWM outputs with  
217 symmetrical waveforms are obtained. As shown in Fig. 6, 218  
only two transitions or less (from low to high or from high  
219 to low) occur on the corresponding PWM outputs within a  
220 sampling period. This fact decreases the switching frequency  
221 of the inverter legs and allows easy DSP implementation. The  
222 switching sequences and the corresponding applying times for  
223 all sectors are presented in Table I. It should also be noticed  
224 that both continuous and discontinuous modulation techniques  
225 can be obtained with this new 24-sector SVPWM scheme. This  
226 is achieved by selecting the appropriate zero voltage vector  
227 locations within the switching sequence. 228

1) *Continuous Modulation C6  $\phi$  SVPWM24*: Continuous  
229 PWM technique (C6  $\phi$  SVPWM24) can be obtained for all sec-  
230 tors by selecting the switching sequences presented in Table I.  
231 As an example, when the reference voltage vector is located  
232 in sector 1, a C6  $\phi$  SVPWM24 is obtained by selecting the  
233 following sequence: 234

$$|56-41-9-11-15-7|7-15-11-9-41-56|.$$

2) *Discontinuous Modulation D6  $\phi$  SVPWM24-B1 and B2*:  
235 Two discontinuous PWM schemes can be obtained through the  
236 appropriate positioning of the zero voltage vectors. In sector 1,  
237 the examples are as follows. 238

1) *D6  $\phi$  SVPWM24-B1*: The first discontinuous modulation  
239 technique can be obtained by placing the zero voltage  
240 vector both at the beginning and at the end of the switch-  
241 ing sequence, as follows: 242

$$|56-41-9-11-15|15-11-9-41-56|.$$

2) *D6  $\phi$  SVPWM24-B2*: The second discontinuous mod-  
243 ulation technique is obtained by placing the zero volt-  
244 age vector in the middle of the switching sequence, as  
245 follows: 246

$$|41-9-11-15-7|7-15-11-9-41|.$$

3) *Switching Sequences and Applying Time Selection*: For  
247 optimal DSP implementation and low algorithm execution time,  
248 the applying times ( $t_1, t_2, t_3$ , and  $t_4$ ) computation can be  
249 simplified by an offline calculation for all sectors in the same  
250 manner as for sector 1. As a result, within each sampling period,  
251 there is a total of only 12 coefficients  $T_i$  to be calculated in (6).  
252

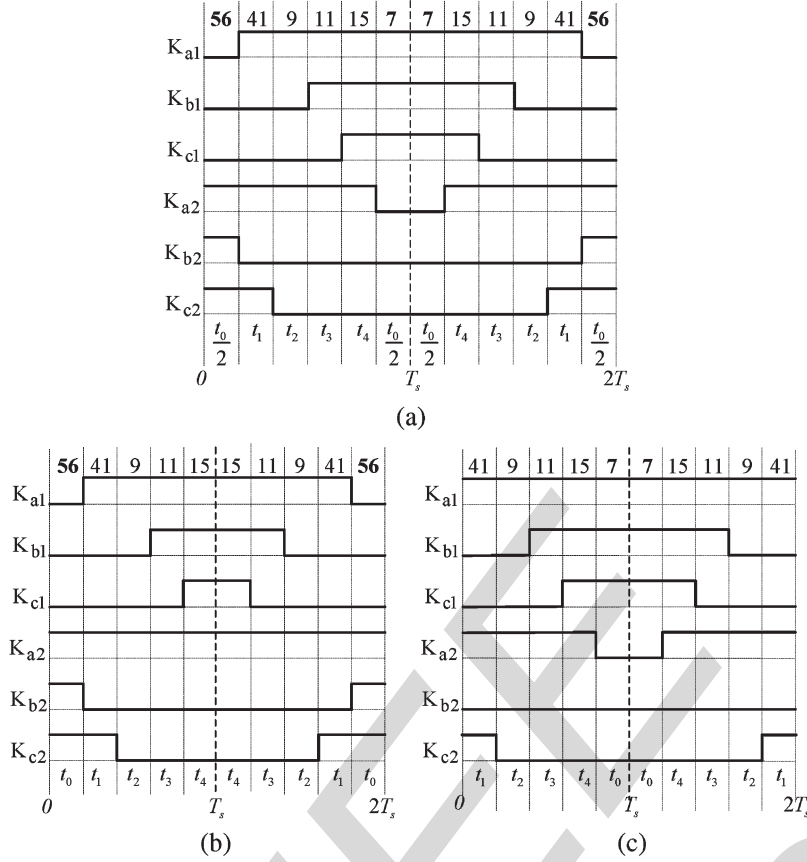


Fig. 6. Twenty-four-sector SVPWM switching sequences when the reference voltage vector is located in sector 1. (a) C6  $\phi$  SVPWM24. (b) D6  $\phi$  SVPWM24-B1. (c) D6  $\phi$  SVPWM24-B2.

Table I describes the C6  $\phi$  SVPWM24 switching sequences and applying time selection according to the sector number in the  $(\alpha-\beta)$  plane.

0.907, coincides with the corresponding value for the three-phase SVPWM [20]. Note that  $m_{\max}$  is obtained by solving  $t_0 = T_s - (t_1 + t_2 + t_3 + t_4) = 0$  as shown in Appendix B.

$$\begin{bmatrix} T_1 \\ T_2 \\ T_3 \\ T_4 \\ T_5 \\ T_6 \\ T_7 \\ T_8 \\ T_9 \\ T_{10} \\ T_{11} \\ T_{12} \end{bmatrix} = \frac{T_s}{2V_{dc}} \begin{bmatrix} \sqrt{3}-2 & 1 \\ 1 & -\sqrt{3} \\ 1 & \sqrt{3}-2 \\ 0 & 2 \\ \sqrt{3}-1 & \sqrt{3}-1 \\ -(\sqrt{3}-1) & \sqrt{3}-1 \\ \sqrt{3} & -1 \\ 1 & -(\sqrt{3}-2) \\ -(\sqrt{3}-2) & 1 \\ 2 & 0 \\ \sqrt{3} & 1 \\ 1 & \sqrt{3} \end{bmatrix} \begin{bmatrix} v_{s\alpha}^* \\ v_{s\beta}^* \end{bmatrix}. \quad (6)$$

#### D. Maximum Modulation Index

The modulation index  $m$  can be defined as the ratio of the fundamental component magnitude of the line to neutral inverter output voltage  $V_{1m}$  to the fundamental component magnitude of the six-step mode voltage  $V_{1m6step} = 2V_{dc}/\pi$  [17]. When the inverter is operating in the linear modulation region, the sum of the applying times of the active voltage vectors is less than the switching period  $T_s$  [18], [19]. The largest value for linear output with the 12-sector and the proposed 24-sector SVPWM techniques,  $m_{\max} = \pi/(2\sqrt{3}) \approx$

#### IV. HARMONIC CURRENT ANALYSIS

The voltage and current waveform quality of the PWM-VSI drives is determined via the switching frequency harmonics, since they determine the switching frequency copper losses and the torque ripple of a motor load and the line current total harmonic distortion of a line-connected VSI. While the copper losses are measured over a fundamental cycle and therefore require a per fundamental cycle (macroscopic) rms ripple current value calculation, the peak and local stresses are properly investigated on a per-carrier cycle (microscopic) basis. Therefore, first a microscopic and then a macroscopic investigation is required [20]. Because, the machine model includes  $(\alpha-\beta)$  and  $(x-y)$  components, the harmonic current analysis must be made for the  $(\alpha-\beta)$  and  $(x-y)$  currents.

##### A. Normalized Harmonic Currents and Fluxes Calculation

The stator voltage equations in the stator coordinate system are expressed as follows:

$$\begin{aligned} v_{s\alpha\beta} &= R_s i_{s\alpha\beta} + \frac{d\lambda_{s\alpha\beta}}{dt} \\ v_{sxy} &= R_s i_{sxy} + L_{lsxy} \frac{di_{sxy}}{dt} \end{aligned} \quad (7)$$

TABLE I  
PROPOSED C6  $\phi$  SVPWM24 SWITCHING SEQUENCES

Sector	Switching sequences	Voltage vectors applying times			
		$t_1$	$t_2$	$t_3$	$t_4$
1	56-41-9-11-15-7	$T_2$	$T_5$	$T_4$	$-T_1$
2	56-57-41-9-11-7	$T_1$	$T_2$	$T_3$	$T_4$
3	0-9-11-27-59-63	$T_7$	$T_9$	$-T_2$	$-T_6$
4	0-8-9-11-27-63	$T_6$	$T_7$	$T_8$	$-T_2$
5	7-11-27-26-24-56	$T_{10}$	$T_1$	$-T_7$	$T_3$
6	7-3-11-27-26-56	$-T_3$	$T_{10}$	$T_5$	$-T_7$
7	63-27-26-18-2-0	$T_{11}$	$T_6$	$-T_{10}$	$T_8$
8	63-31-27-26-18-0	$-T_8$	$T_{11}$	$T_9$	$-T_{10}$
9	56-26-18-22-23-7	$T_{12}$	$-T_3$	$-T_{11}$	$T_5$
10	56-58-26-18-22-7	$-T_5$	$T_{12}$	$T_1$	$-T_{11}$
11	0-18-22-54-62-63	$T_4$	$-T_8$	$-T_{12}$	$T_9$
12	0-16-18-22-54-63	$-T_9$	$T_4$	$T_6$	$-T_{12}$
13	7-22-54-52-48-56	$-T_2$	$-T_5$	$-T_4$	$T_1$
14	7-6-22-54-52-56	$-T_1$	$-T_2$	$-T_3$	$-T_4$
15	63-54-52-36-4-0	$-T_7$	$-T_9$	$T_2$	$T_6$
16	63-55-54-52-36-0	$-T_6$	$-T_7$	$-T_8$	$T_2$
17	56-52-36-37-39-7	$-T_{10}$	$-T_1$	$T_7$	$-T_3$
18	56-60-52-36-37-7	$T_3$	$-T_{10}$	$-T_5$	$T_7$
19	0-36-37-45-61-63	$-T_{11}$	$-T_6$	$T_{10}$	$-T_8$
20	0-32-36-37-45-63	$T_8$	$-T_{11}$	$-T_9$	$T_{10}$
21	7-37-45-41-40-56	$-T_{12}$	$T_3$	$T_{11}$	$-T_5$
22	7-5-37-45-41-56	$T_5$	$-T_{12}$	$-T_1$	$T_{11}$
23	63-45-41-9-1-0	$-T_4$	$T_8$	$T_{12}$	$-T_9$
24	63-47-45-41-9-0	$T_9$	$-T_4$	$-T_6$	$T_{12}$

where the stator and the rotor flux equations are given by:

$$\begin{aligned}\lambda_{s\alpha\beta} &= L_s i_{s\alpha\beta} + M i_{r\alpha\beta} \\ \lambda_{r\alpha\beta} &= L_r i_{r\alpha\beta} + M i_{s\alpha\beta}.\end{aligned}\quad (8)$$

The stator flux equation can be rewritten as:

$$\lambda_{s\alpha\beta} = \sigma L_s i_{s\alpha\beta} + \frac{M}{L_r} \lambda_{r\alpha\beta}.\quad (9)$$

Substituting (9) in (7), the stator voltage equation can be expressed as follows:

$$v_{s\alpha\beta} = R_s i_{s\alpha\beta} + \sigma L_s \frac{di_{s\alpha\beta}}{dt} + \frac{M}{L_r} \frac{d\lambda_{r\alpha\beta}}{dt}.\quad (10)$$

If only the harmonic voltages and currents are considered, it will be assumed that the reference voltage vector  $v_{s\alpha\beta}^*$  is constant over the switching period  $T_s$ , because the switching frequency  $f_s$  is much higher than the fundamental frequency  $f_e$ , and that the stator and the rotor time constants are much larger than the switching period, with the resistance drops being neglected [21]. Under these assumptions, the voltages and

currents can be separated in the harmonic components, which change over  $T_s$  while the fundamental components remain constant over the same period. Thus, from (7) and (10), the harmonic voltage equations can be expressed as follows:

$$\begin{aligned}\tilde{v}_{s\alpha\beta} &= \sigma L_s \frac{d\tilde{i}_{s\alpha\beta}}{dt} \\ \tilde{v}_{sxy} &= L_{lsxy} \frac{d\tilde{i}_{sxy}}{dt}\end{aligned}\quad (11)$$

where  $\tilde{v}_{s\alpha\beta}$  is the harmonic voltage and is equal to the difference between the actual voltage vector and the reference vector  $v_{s\alpha\beta}^*$ .

Assuming that the instantaneous harmonic currents are zero at the beginning and at the end of the carrier cycle, the  $(\alpha-\beta)$  and  $(x-y)$  harmonic stator currents per-carrier cycle can be calculated as follows [20], [22], [23]:

$$\begin{aligned}\tilde{i}_{s\alpha\beta} &= \frac{1}{\sigma L_s} \int_{NT_s}^{(N+1)T_s} (V_{s\alpha\beta k} - v_{s\alpha\beta}^*) dt \\ \tilde{i}_{sxy} &= \frac{1}{L_{lsxy}} \int_{NT_s}^{(N+1)T_s} (V_{sxy k}) dt.\end{aligned}\quad (12)$$

In (12),  $V_{s\alpha\beta k}$  and  $V_{sxy k}$  are the inverter output voltage vectors of the  $k$ th state. They change according to the selected switching sequence, since for high  $f_s/f_e$  values, the  $v_{s\alpha\beta}^*$  term can be assumed as constant within a carrier cycle. Thus, the above integral can be calculated in a closed form.

Because the harmonic current and harmonic flux are only different in scale, and in order to eliminate the need for load parameters in (12), the harmonic flux trajectories can be investigated. Nevertheless, the  $(x-y)$  current components are limited by the stator leakage inductance  $L_{lsxy}$ , which depends on the coil pitch of the stator windings [10]. Consequently, the harmonic characteristics of the VSI feeding DSIM should be investigated with the introduction of the coefficient  $k_{\sigma xy} = \sigma L_s / L_{lsxy}$ , which is necessary to evaluate and compare the performances of the PWM techniques. So, employing (12) and normalizing with respect to  $\lambda_b$ , the per-carrier cycle rms value of the normalized harmonic current can be calculated with:

$$\begin{aligned}\tilde{i}_{srms}^2(m, \theta) &= \left(\frac{\lambda_b}{\sigma L_s}\right)^2 \frac{1}{T_s} \int_{NT_s}^{(N+1)T_s} (\tilde{\lambda}_{s\alpha\beta}^2 + k_{\sigma xy}^2 \tilde{\lambda}_{sxy}^2) dt \\ &= \left(\frac{\lambda_b}{\sigma L_s}\right)^2 (\tilde{\lambda}_{s\alpha\beta rms}^2(m, \theta) + k_{\sigma xy}^2 \tilde{\lambda}_{sxy rms}^2(m, \theta)) \\ &= \left(\frac{\lambda_b}{\sigma L_s}\right)^2 (\tilde{\lambda}_{srms}^2(m, \theta))\end{aligned}\quad (13)$$

where  $\lambda_b = 2\sqrt{3}V_{dc}T_s/\pi$ ,  $\tilde{\lambda}_{s\alpha\beta} = \sigma L_s \tilde{i}_{s\alpha\beta}$ , and  $\tilde{\lambda}_{sxy} = L_{lsxy} \tilde{i}_{sxy}$

TABLE II  
SWITCHING FREQUENCY REDUCTION COEFFICIENT

N°	SVPWM Techniques	$k_f$	$f_s$
1	C6 $\phi$ SVPWM12	1	$f_s = \frac{1}{k_f} \cdot f_{sw}$
2	D6 $\phi$ SVPWM12-A	2/3	
3	D6 $\phi$ SVPWM12-B1	1/2	
4	D6 $\phi$ SVPWM12-B2	5/12	
5	C6 $\phi$ SVPWM24	1	
6	D6 $\phi$ SVPWM24-B1	5/6	
7	D6 $\phi$ SVPWM24-B2	2/3	

The per-fundamental cycle rms value of the harmonic current determines the waveform quality and harmonic losses. Averaging (13) over a fundamental period results in the global harmonic current calculation as follows:

$$\begin{aligned}
 \tilde{I}_{sfrms}^2(m) &= \left( \frac{\lambda_b}{\sigma L_s} \right)^2 \frac{1}{2\pi} \int_{2\pi} \tilde{\lambda}_{sfrms}^2(m, \theta) d\theta \\
 &= \left( \frac{\lambda_b}{\sigma L_s} \right)^2 \left( \tilde{\lambda}_{s\alpha\beta frms}^2(m) + k_{\sigma xy}^2 \tilde{\lambda}_{sxy frms}^2(m) \right) \\
 &= \left( \frac{\lambda_b}{\sigma L_s} \right)^2 \tilde{\lambda}_{sfrms}^2(m). \quad (14)
 \end{aligned}$$

The above integral yields a polynomial function of the modulation index  $m$ . As an example, the per-fundamental cycle rms normalized harmonic flux  $\tilde{\lambda}_{sfrms}$  was calculated for all the discussed PWM techniques. This results in  $m$  dependent analytical formulas summarized in Appendix C.

#### B. Performance Comparison

For comparison purposes, the harmonic current analysis is performed at the same average switching frequency  $f_{sw}$  for all the PWM techniques. Therefore, a switching frequency reduction coefficient  $k_f$  is introduced for each PWM technique according to Table II. This coefficient can be determined from the ratio of the discontinuous to the continuous PWM techniques regarding the number of commutations of all legs during one sampling period. The curves of the per-fundamental cycle normalized rms harmonic flux for all the discussed PWM techniques have been plotted as a function of modulation index  $m$ , as shown in Fig. 7. It is clear that the rms value of the harmonic flux varies with the PWM technique used and according to the selected switching sequences. These curves show that the D6  $\phi$  SVPWM12-A has practically the best performance at a low modulation index range, while the D6  $\phi$  SVPWM12-B1-B2 exhibits the best performance in the high modulation index range. However, as the modulation index increases, the C6  $\phi$  SVPWM12 performance rapidly degrades compared to the C6  $\phi$  SVPWM24 of the proposed 24-sector PWM scheme, which reveals excellent performance over the whole voltage range. While the D6  $\phi$  SVPWM24-B1-B2 PWM strategies present harmonic characteristics similar to the ones obtained with the D6  $\phi$  SVPWM12-A-B1 and B2 strategies, the

proposed 24-sector PWM techniques allow a sampling frequency increase and as a result, the switching frequency can be increased by a factor of two as compared to the 12-sector PWMs. Therefore, significant harmonic current reductions can be achieved as shown in Fig. 7(h) for the worst case, when  $k_{\sigma xy} = 10$ .

It should be noted that discontinuous PWM techniques allow a higher sampling rate selection and can be applied in a high voltage range, while continuous ones are advantageous in the low voltage range. In addition, an optimal PWM scheme can be obtained with a transition between these SVPWM strategies to allow rms harmonic current minimization over the whole voltage range. The intersection points define the optimal transition between different PWM techniques.

Finally, a careful look at D6  $\phi$  SVPWM12-B1 in Fig. 4(c) shows that during one switching period  $T_s$ , two inverter legs have commutations twice. D6  $\phi$  SVPWM12-B2 in Fig. 4(d) shows that one inverter leg has commutations twice. This is never the case for D6  $\phi$  SVPWM24-B1 and B2. Therefore, 12-sector discontinuous PWMs have a maximum instantaneous switching frequency twice as big as in the case of 24-sector discontinuous PWMs. This fact has an impact on inverter switching losses [14], [20]. While it is not the aim of this paper to evaluate the performance of PWM techniques in terms of inverter switching and conduction losses, it can be expected that the 24-sector discontinuous PWMs will have a better performance than the 12-sector ones. Further works on switching and conduction losses are in progress and will be reported in a subsequent paper.

## V. EXPERIMENTAL RESULTS

To confirm the feasibility of the proposed SVPWM techniques over the entire voltage range under  $V/f$  control, a set of experiments are carried out. The experimental test bench (Fig. 8) is composed of a six-phase VSI feeding a 15 kW DSIM prototype, and the whole control algorithm is tested on a dSPACE DS1104 controller board. The original 320F240 firmware does not allow the change in PWM compare registers and action registers many times during a period. So, to allow four changes within PWM period  $T_s$ , the flashed firmware is reprogrammed [15], [24]. Hence, it is possible to implement the 12-sector PWM techniques.

On the contrary, for the proposed 24-sector PWM strategies, usually at most two transitions (from low to high or from high to low) occur symmetrically on the corresponding PWM outputs within a sampling period. This allows easier DSP implementation. Then the original 320F240 firmware is used with the help of specially developed user functions that allow the synchronization of six full PWM and three simple PWM simultaneously on the DS1104 DSP board.

These PWM techniques are successfully tested and the following conclusions can be drawn from these experimental results: In the case of the 12-sector PWM strategies, usually more than two transitions (from low to high or from high to low) occur on the corresponding PWM outputs. This increases the switching frequency of the inverter legs and complicates the experimental test. However, the number of transitions



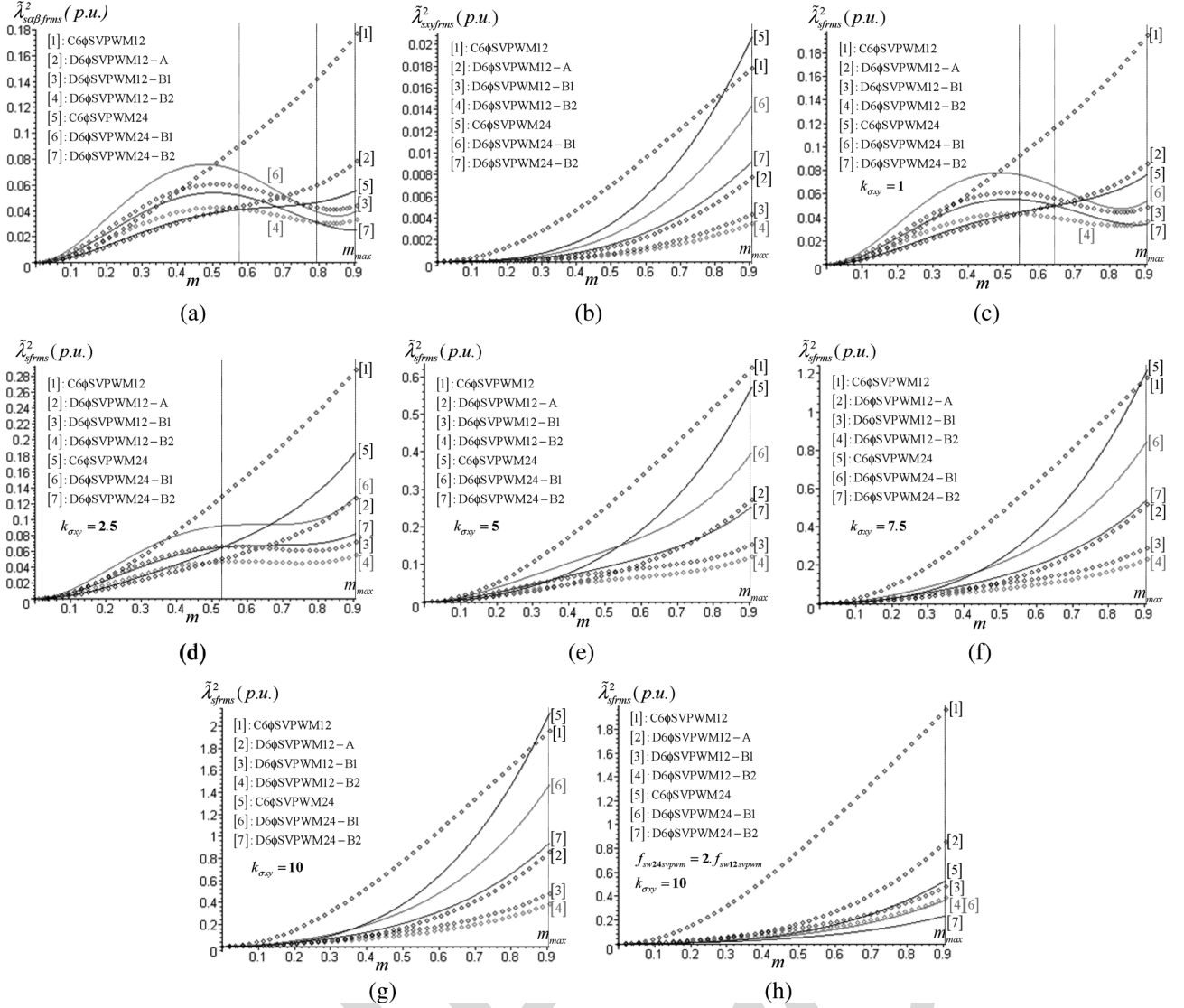


Fig. 7. Per fundamental cycle normalized rms harmonic flux as a function of modulation index  $m$ , for all the discussed PWM techniques. (a)  $(\alpha-\beta)$  rms harmonic flux. (b)  $(x-y)$  rms harmonic flux. (c), (d), (e), (f), (g) RMS harmonic flux at different leakage coupling ( $k_{\sigma xy} = 1; 2.5; 5; 7.5; 10$ ), at the same average switching frequency  $f_{sw}$ . (h) RMS harmonic flux with  $k_{\sigma xy} = 10$ , at  $f_s = 2 \cdot f_{sw}$  for the proposed 24-sector PWM techniques.

on the corresponding PWM outputs is reduced in the case of the proposed 24-sector PWM strategies, which decrease the switching frequency of the inverter legs and allow easy DSP implementation. In addition, for discontinuous PWM techniques, at least two PWM outputs remain unchanged during the entire sampling period. Therefore, the carrier frequency can be increased with harmonic losses reduction.

Experimental results under constant  $V/f$  control, for the cases of C6  $\phi$  SVPWM12, D6  $\phi$  SVPWM12-B2, C6  $\phi$  SVPWM24, and D6  $\phi$  SVPWM24-B2 techniques are presented in Fig. 9. The average switching frequency is set to  $f_{sw} = 5$  kHz and the motor is running at 735 r/min with a connected load. As expected, these SVPWM techniques allow the control of the  $(\alpha-\beta)$  and  $(x-y)$  current components simultaneously.

However, these experimental results demonstrate that the continuous PWM techniques produce a larger amplitude of the harmonic currents in the  $(x-y)$  plane as compared to the discontinuous ones where the amplitude of these currents

is minimized. Moreover, the phase current presents a pure sinusoidal shape and the trajectory of the  $(\alpha-\beta)$  stator current components is a circle for all these PWM techniques, confirming that these currents are controlled as well as  $(x-y)$  harmonic currents. Indeed, it should be remembered that the carrier frequency can be increased by a factor of two for a 50% reduction of harmonic losses in the case of C6  $\phi$  SVPWM24, or by a factor three for a 66% reduction in harmonic losses with the D6  $\phi$  SVPWM24-B2 technique. In addition, due to the simplicity and regularity of the proposed 24-sector PWM techniques, low-cost DSPs for motor control may easily be used.

## VI. CONCLUSION

In this paper, a new SVPWM technique based on the vector space decomposition suitable for six-phase VSI-fed DSIM has been presented. The switching sequences presented lead to continuous and discontinuous modulation strategies, according

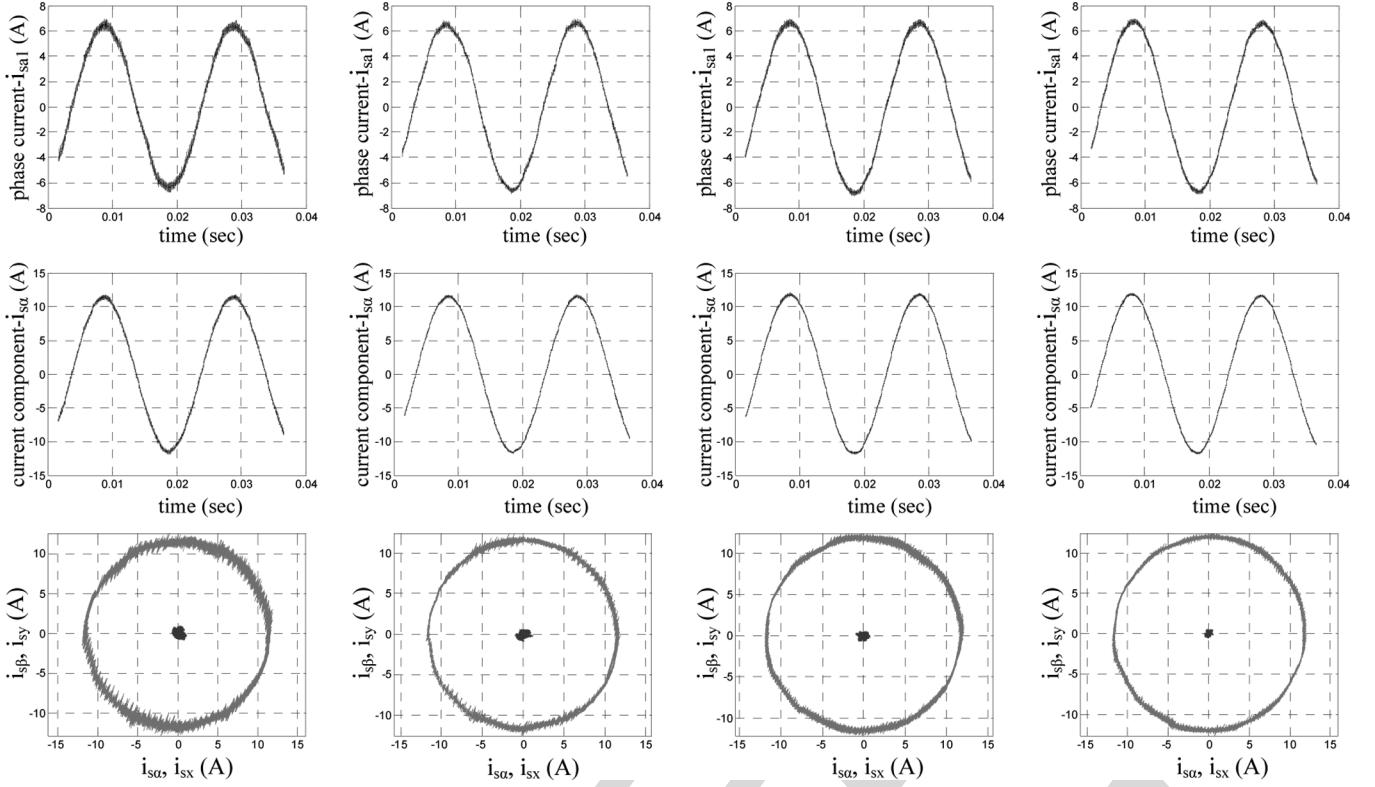


Fig. 8. Experimental test bench.

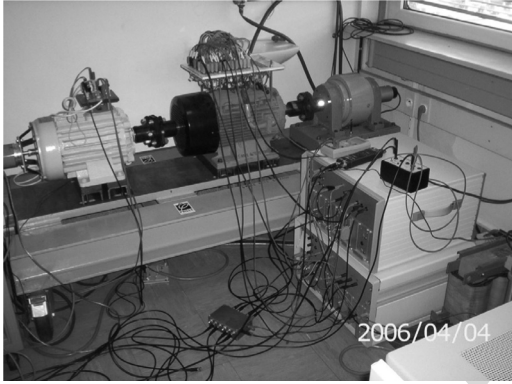


Fig. 9. Experimental results of the SVPWM techniques with the motor operating under a constant  $V/f$  control with connected load for  $f_e = 50$  Hz, at 735 r/min and for the same average switching frequency  $f_{sw}$ . From top to bottom:  $i_{sa1}$  phase current,  $i_{s\alpha}$  current component,  $(\alpha-\beta)$  and  $(x-y)$  plane current trajectories. From left to right: C6  $\phi$  SVPWM12, D6  $\phi$  SVPWM12-B2, C6  $\phi$  SVPWM24, and D6  $\phi$  SVPWM24-B2.

453 to the position of zero voltage vectors during each sampling  
454 period. It is shown that the harmonic current rms values vary  
455 according to the selected switching sequence and the voltage  
456 range. Likewise, from this point of view, the continuous PWM  
457 technique has an advantage in the low and medium voltage  
458 range, while the discontinuous PWM strategy is advantageous  
459 in the high voltage range. Thus, the combination of these  
460 strategies provides the best harmonic current performance over  
461 the whole voltage range. It has been demonstrated that the pro-  
462 posed 24-sector SVPWM techniques, while easy to implement  
463 digitally, allow a switching frequency increase with significant  
464 extra stator harmonic currents reduction.

## APPENDIX A

## VOLTAGE VECTORS APPLYING TIMES CALCULATION

The inverter output voltage vectors are represented in Figs. 3, 467  
and Fig. 5 by decimal number  $k$  equivalent to the binary number 468  
formed by the instantaneous values of the switching functions 469  
defined as: 470

$$k = K_{a1} \times 2^0 + K_{b1} \times 2^1 + K_{c1} \times 2^2 + K_{a2} \times 2^3 + K_{b2} \times 2^4 + K_{c2} \times 2^5. \quad (A1)$$

The instantaneous values of the six-phase VSI output voltage 471  
vectors ( $v_{a1}, v_{b1}, v_{c1}, v_{a2}, v_{b2}, v_{c2}$ ) can be determined by using 472  
the inverter connection matrix  $[Mc]$  as follows: 473

$$[v_{a1} \ v_{b1} \ v_{c1} \ v_{a2} \ v_{b2} \ v_{c2}]^T = [Mc][K_{a1} \ K_{b1} \ K_{c1} \ K_{a2} \ K_{b2} \ K_{c2}]^T \quad (A2)$$

where

$$[Mc] = \frac{V_{dc}}{3} \begin{bmatrix} 2 & -1 & -1 & 0 & 0 & 0 \\ -1 & 2 & -1 & 0 & 0 & 0 \\ -1 & -1 & 2 & 0 & 0 & 0 \\ 0 & 0 & 0 & 2 & -1 & -1 \\ 0 & 0 & 0 & -1 & 2 & -1 \\ 0 & 0 & 0 & -1 & -1 & 2 \end{bmatrix}. \quad (A3)$$

The inverter output voltage vectors are transformed into 475  
 $(\alpha-\beta)$ ,  $(x-y)$ , and  $(o_1-o_2)$  planes by means of the transfor- 476  
mation matrix  $[Ts]^{-1}$  given in (1), as: 477

$$[v_{s\alpha k} \ v_{s\beta k} \ v_{sxk} \ v_{syk} \ v_{o1k} \ v_{o2k}]^T = [Ts]^{-1}[v_{a1} \ v_{b1} \ v_{c1} \ v_{a2} \ v_{b2} \ v_{c2}]^T \quad (A4)$$

For example, when the reference voltage vector is located in sector 1, voltage vectors 41, 9, 11, and 15 are selected and their equivalent binary numbers are defined as:

$$\begin{aligned} 41 &= [1 \ 0 \ 1|0 \ 0 \ 1] \\ 9 &= [0 \ 0 \ 1|0 \ 0 \ 1] \\ 11 &= [0 \ 0 \ 1|0 \ 1 \ 1] \\ 15 &= [0 \ 0 \ 1|1 \ 1 \ 1]. \end{aligned} \quad (A5)$$

Then the  $(\alpha-\beta)$ , and  $(x-y)$  voltages can be calculated by using (A2), and (A4), as follows:

$$\begin{aligned} &\begin{bmatrix} V_{s\alpha 41} & V_{s\alpha 9} & V_{s\alpha 11} & V_{s\alpha 15} \\ V_{s\beta 41} & V_{s\beta 9} & V_{s\beta 11} & V_{s\beta 15} \\ V_{sx 41} & V_{sx 9} & V_{sx 11} & V_{sx 15} \\ V_{sy 41} & V_{sy 9} & V_{sy 11} & V_{sy 15} \end{bmatrix} \\ &= \frac{V_{dc}}{2\sqrt{3}} \begin{bmatrix} 2+\sqrt{3} & 2+\sqrt{3} & 1+\sqrt{3} & \sqrt{3} \\ -1 & 1 & 1+\sqrt{3} & 1 \\ 2-\sqrt{3} & 2-\sqrt{3} & 1-\sqrt{3} & -\sqrt{3} \\ -1 & 1 & 1-\sqrt{3} & 1 \end{bmatrix}. \end{aligned} \quad (A6)$$

The voltage vectors applying times:  $t_1$ ,  $t_2$ ,  $t_3$  and  $t_4$  are obtained as:

$$\begin{aligned} \begin{bmatrix} t_1 \\ t_2 \\ t_3 \\ t_4 \end{bmatrix} &= \begin{bmatrix} V_{s\alpha 41} & V_{s\alpha 9} & V_{s\alpha 11} & V_{s\alpha 15} \\ V_{s\beta 41} & V_{s\beta 9} & V_{s\beta 11} & V_{s\beta 15} \\ V_{sx 41} & V_{sx 9} & V_{sx 11} & V_{sx 15} \\ V_{sy 41} & V_{sy 9} & V_{sy 11} & V_{sy 15} \end{bmatrix}^{-1} \begin{bmatrix} v_{s\alpha}^* T_s \\ v_{s\beta}^* T_s \\ v_{sx}^* T_s \\ v_{sy}^* T_s \end{bmatrix} \\ t_0 &= T_s - (t_1 + t_2 + t_3 + t_4). \end{aligned} \quad (A7)$$

Substituting (A6) in (A7), the applying times can be calculated as follows:

$$\begin{aligned} \begin{bmatrix} t_1 \\ t_2 \\ t_3 \\ t_4 \end{bmatrix} &= \frac{T_s}{2V_{dc}} \begin{bmatrix} 1 & -\sqrt{3} & -1 & -\sqrt{3} \\ \sqrt{3}-1 & \sqrt{3}-1 & \sqrt{3}+1 & \sqrt{3}+1 \\ 0 & 2 & 0 & v-2 \\ -(\sqrt{3}-2) & -1 & -(\sqrt{3}+2) & 1 \end{bmatrix} \begin{bmatrix} v_{s\alpha}^* \\ v_{s\beta}^* \\ v_{sx}^* \\ v_{sy}^* \end{bmatrix}. \end{aligned} \quad (A8)$$

With  $v_{sx}^* = v_{sy}^* = 0$ , (A8) can be written as:

$$\begin{aligned} \begin{bmatrix} t_1 \\ t_2 \\ t_3 \\ t_4 \end{bmatrix} &= \frac{T_s}{2V_{dc}} \begin{bmatrix} 1 & -\sqrt{3} \\ \sqrt{3}-1 & \sqrt{3}-1 \\ 0 & 2 \\ -(\sqrt{3}-2) & -1 \end{bmatrix} \begin{bmatrix} v_{s\alpha}^* \\ v_{s\beta}^* \end{bmatrix} = \begin{bmatrix} T_2 \\ T_5 \\ T_4 \\ -T_1 \end{bmatrix}. \end{aligned} \quad (A9)$$

## APPENDIX B

### MAXIMUM MODULATION INDEX CALCULATION

The maximum modulation index  $m_{\max}$  can be obtained by solving  $t_0 = T_s - (t_1 + t_2 + t_3 + t_4) = 0$ . For example in sector 1, the sum of the applying times of the active voltage vectors is calculated from (A9) as:

$$\theta \in \left[0, \frac{\pi}{12}\right] \quad t_1 + t_2 + t_3 + t_4 = \frac{T_s}{V_{dc}} v_{s\alpha}^* \quad (B1)$$

where  $v_{s\alpha}^* = \sqrt{3}V_{1m} \cos(\theta)$ ,  $v_{s\beta}^* = \sqrt{3}V_{1m} \sin(\theta)$

$$V_{1m} = mV_{1m6step} = m2V_{dc}/\pi.$$

When

$$t_0 = 0 : T_s = t_1 + t_2 + t_3 + t_4 = 2\sqrt{3}\frac{T_s}{\pi}m \cos(\theta) \quad (B2)$$

From (B2), the modulation index equation can be given as:

$$m = \frac{\pi}{2\sqrt{3} \cos(\theta)}. \quad (B3)$$

To determine the angle  $\theta$  corresponding to  $m_{\max}$ , (B3) is derived:

$$\frac{dm}{d\theta} = \frac{\pi \sin(\theta)}{2\sqrt{3} \cos^2(\theta)}. \quad (B4)$$

Equation (B4) is solved for  $\theta = 0$ . Thus, replacing  $\theta$  in (B3):

$$m_{\max} = \frac{\pi}{2\sqrt{3} \cos(0)} = \frac{\pi}{2\sqrt{3}} \approx 0.907. \quad (B5)$$

## APPENDIX C

### ANALYTICAL FORMULAS OF THE RMS HARMONIC FLUX

The per-fundamental cycle rms normalized harmonic flux  $\tilde{\lambda}_{sfrms}$  was calculated for all the discussed PWM techniques. Only the analytical formulas of the proposed 24-sector PWMs are presented here and the ones of the 12-sector PWMs can be found in [10]. These formulas are given below.

#### A. Continuous Modulation C6 $\phi$ SVPWM24

$$\begin{aligned} \tilde{\lambda}_{s\alpha\beta frms}^2(m) &= \frac{1}{48}m^2 + \frac{1}{144\pi^2} \\ &\times (56\sqrt{3} + 63\sqrt{6} - 57\sqrt{2} - 228)m^3 \\ &+ \frac{1}{32\pi^3}(24\pi + 27 - 21\sqrt{3} - 8\sqrt{3}\pi)m^4 \\ \tilde{\lambda}_{sxy frms}^2(m) &= \frac{1}{144\pi^2}(63\sqrt{6} + 18 - 52\sqrt{3} - 57\sqrt{2})m^3. \end{aligned} \quad (C1)$$

#### B. Discontinuous Modulation D6 $\phi$ SVPWM24-B1

$$\begin{aligned} \tilde{\lambda}_{s\alpha\beta frms}^2(m) &= \frac{25}{432}m^2 - \frac{25}{5184\pi^2} \\ &\times (633\sqrt{2} + 408 - 56\sqrt{3} - 387\sqrt{6})m^3 \\ &- \frac{25}{576\pi^3}(15\sqrt{3} + 8\sqrt{3}\pi - 24\pi - 45)m^4 \\ \tilde{\lambda}_{sxy frms}^2(m) &= \frac{25}{5184\pi^2}(63\sqrt{6} + 18 - 52\sqrt{3} - 57\sqrt{2})m^3. \end{aligned} \quad (C2)$$

#### C. Discontinuous Modulation D6 $\phi$ SVPWM24-B2

$$\begin{aligned} \tilde{\lambda}_{s\alpha\beta frms}^2(m) &= \frac{1}{27}m^2 - \frac{1}{324\pi^2} \\ &\times (129\sqrt{2} + 45\sqrt{6} + 48 - 56\sqrt{3})m^3 \\ &+ \frac{1}{6\pi^3}(2\pi + 3 - \sqrt{3})m^4 \\ \tilde{\lambda}_{sxy frms}^2(m) &= \frac{1}{324\pi^2}(63\sqrt{6} + 18 - 52\sqrt{3} - 57\sqrt{2})m^3. \end{aligned} \quad (C3)$$

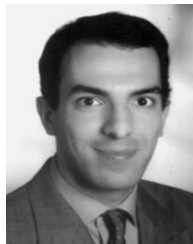
## REFERENCES

- 510
- 511 [1] V. T. Somasekhar, K. Gopakumar, M. R. Baiju, K. K. Mohapatra, and  
512 L. Umanand, "A multilevel inverter system for an induction motor with  
513 open-end windings," *IEEE Trans. Ind. Electron.*, vol. 52, no. 3, pp. 824–  
514 836, Jun. 2005.
- 515 [2] R. C. Portillo *et al.*, "Modeling strategy for back-to-back three-level con-  
516 verters applied to high-power wind turbines," *IEEE Trans. Ind. Electron.*,  
517 vol. 53, no. 5, pp. 1483–1491, Oct. 2006.
- 518 [3] A. K. Gupta and A. M. Khambadkone, "A space vector PWM scheme for  
519 multilevel inverters based on two-level space vector PWM," *IEEE Trans.*  
520 *Ind. Electron.*, vol. 53, no. 5, pp. 1631–1639, Oct. 2006.
- 521 [4] K. Hatua and V. T. Ranganathan, "Direct torque control schemes for  
522 split-phase induction machine," *IEEE Trans. Ind. Appl.*, vol. 41, no. 5,  
523 pp. 1243–1254, Sep./Oct. 2005.
- 524 [5] Y. Zhao and T. A. Lipo, "Space vector PWM control of dual three-phase  
525 induction machine using vector space decomposition," *IEEE Trans. Ind.*  
526 *Appl.*, vol. 31, no. 5, pp. 1100–1109, Sep./Oct. 1995.
- 527 [6] M. A. Abbas, R. Christen, and T. M. Jahns, "Six-phase voltage source  
528 inverter driven induction motor," *IEEE Trans. Ind. Appl.*, vol. 1A-20, no. 5,  
529 pp. 1251–1259, Sep./Oct. 1984.
- 530 [7] D. Hadiouche, H. Razik, and A. Rezzoug, "On the modeling and design  
531 of dual-stator windings to minimize circulating harmonic currents for VSI  
532 fed AC machines," *IEEE Trans. Ind. Appl.*, vol. 40, no. 2, pp. 506–515,  
533 Mar./Apr. 2004.
- 534 [8] A. R. Muñoz and T. A. Lipo, "Dual stator winding induction machine  
535 drive," *IEEE Trans. Ind. Appl.*, vol. 36, no. 5, pp. 1369–1379,  
536 Sep./Oct. 2000.
- 537 [9] K. Gopakumar, V. T. Ranganathan, and S. R. Bhat, "Split-phase induction  
538 motor operation from PWM voltage source inverter," *IEEE Trans. Ind.*  
539 *Appl.*, vol. 29, no. 5, pp. 927–932, Sep./Oct. 1993.
- 540 [10] D. Hadiouche, L. Baghli, and A. Rezzoug, "Space vector PWM  
541 techniques for dual three-phase AC machine: Analysis, performance  
542 evaluation, and DSP implementation," *IEEE Trans. Ind. Appl.*, vol. 42,  
543 no. 4, pp. 1112–1122, Jul./Aug. 2006.
- 544 [11] R. Bojoi, M. Lazzari, F. Profumo, and A. Tenconi, "Digital field-oriented  
545 control for dual three-phase induction motor drives," *IEEE Trans. Ind.*  
546 *Appl.*, vol. 39, no. 3, pp. 752–760, May/Jun. 2003.
- 547 [12] K. K. Mohapatra, R. S. Kanchan, M. R. Baiju, P. N. Tekwani, and  
548 K. Gopakumar, "Independent field-oriented control of two split-phase  
549 induction motors from a single six-phase inverter," *IEEE Trans. Ind.*  
550 *Electron.*, vol. 52, no. 5, pp. 1372–1382, Oct. 2005.
- 551 [13] W. Tiejun, G. Chenglin, C. Yongbing, and J. Xiaoyi, "Research on har-  
552 monics of multiphase induction motors," in *Proc. IEEE IEMDC*, Antalya,  
553 Turkey, May 3–5, 2007, vol. 2, pp. 1524–1528.
- 554 [14] J. W. Kolar, H. Ertl, and F. C. Zach, "Influence of the modulation method  
555 on the conduction and switching losses of a PWM converter system,"  
556 *IEEE Trans. Ind. Appl.*, vol. 27, no. 6, pp. 1063–1075, Nov./Dec. 1991.
- 557 [15] K. Marouani, L. Baghli, D. Hadiouche, A. Kheloui, and A. Rezzoug,  
558 "Discontinuous SVPWM techniques for double star induction motor  
559 drive control," in *Proc. IEEE IECON*, Paris, France, Nov. 6–10, 2006,  
560 pp. 902–907.
- 561 [16] G. K. Singh, K. Nam, and S. K. Lim, "A simple indirect field-oriented  
562 control scheme for multiphase induction machine," *IEEE Trans. Ind.*  
563 *Electron.*, vol. 52, no. 4, pp. 1177–1184, Aug. 2005.
- 564 [17] D. C. Lee and G. M. Lee, "Linear control of inverter output voltage in  
565 overmodulation," *IEEE Trans. Ind. Electron.*, vol. 44, no. 4, pp. 590–592,  
566 Aug. 1997.
- 567 [18] S. R. Bowes and Y. S. Lai, "The relationship between space-vector mod-  
568 ulation and regular-sampled PWM," *IEEE Trans. Ind. Electron.*, vol. 44,  
569 no. 5, pp. 670–679, Oct. 1997.
- 570 [19] O. Ojo, "The generalized discontinuous PWM scheme for three-phase  
571 voltage source inverters," *IEEE Trans. Ind. Electron.*, vol. 51, no. 6,  
572 pp. 1280–1289, Dec. 2004.
- 573 [20] A. M. Hava, R. J. Kerkman, and T. A. Lipo, "Simple analytical and graph-  
574 ical methods for carrier-based PWM-VSI drives," *IEEE Trans. Power*  
575 *Electron.*, vol. 14, no. 1, pp. 49–61, Jan. 1999.
- 576 [21] S. Ogasawara, H. Akagi, and A. Nabae, "A novel PWM scheme of voltage  
577 source inverters based on space vector theory," in *Proc. EPE*, Aachen,  
578 Germany, Oct. 1989, pp. 1197–1202.
- 579 [22] H. W. van der Broeck, H. C. Skudelny, and G. V. Stanke, "Analysis and  
580 realization of a pulsewidth modulator based on voltage space vectors,"  
581 *IEEE Trans. Ind. Appl.*, vol. 24, no. 1, pp. 142–150, Jan./Feb. 1988.
- 582 [23] J. Holtz and B. Beyer, "Optimal pulse width modulation for AC servos  
583 and low-cost industrial drives," *IEEE Trans. Ind. Appl.*, vol. 30, no. 4,  
584 pp. 1039–1047, Jul./Aug. 1994.
- 585 [24] *TMS320F/C240 DSP Controllers Reference Guide, Peripheral and Spe-*  
586 *cific Devices*, Texas Instruments, Dallas, TX, 1999. Literature Number  
587 SPRU161C.



**Khoudir Marouani** was born in 1972. He received the Degree of Engineer in automatics and the Degree of Magister in electrical engineering from the Polytechnic Military School (EMP), Algiers, Algeria, in 1996 and 2000, respectively, where he is currently working toward the Ph.D. degree in the Electrical Engineering Laboratory.

He is currently working as a Research and Teaching Assistant with the Electrical Engineering Laboratory, EMP. His research interests include power electronics, electrical drives and active power filters.



**Lotfi Baghli** was born in 1971. He received the Electrical Engineering Diploma degree (with honors) from the Ecole Nationale Polytechnique, Algiers, Algeria, in 1989, and the DEA degree in electrical engineering from the Université Henri Poincaré, Nancy, France, in 1995 and 1999, respectively.

He is currently a Lecturer at IUFM de Lorraine and a member of Groupe de Recherche en Electrotechnique et Electronique de Nancy, Nancy. His works concern digital control using DSP, PSO and genetic algorithms applied to the control and identification of electrical machines.



**Djafar Hadiouche** was born in 1974. He received the Ph.D. degree in electrical engineering from the University Henri Poincaré, Nancy, France, in 2001.

Until 2002, he was Assistant Lecturer in the same university and did research in the laboratory of the "Groupe de Recherche en Electrotechnique et Electronique de Nancy," Nancy. Since 2003, he has been a Motion Specialist Engineer with GE Fanuc Automation Solutions Europe, Echternach, Luxembourg. His main tasks include servosizing, tools and motion programs development, electronic cam profiling and motion technical training. His main research interests concern multiphase ac machines, their modeling, identification, pulsewidth modulation techniques, and vector control.

Dr. Hadiouche received the Best Prize Paper Award from the Electric Machine Committee at the 2001 IEEE IAS Annual Meeting.



**Abdelaziz Kheloui** was born in 1969. He received the M.Sc.Eng. degree from the Ecole Nationale d'ingénieurs et Techniciens d'Algérie, Algiers, Algeria, in 1990, and the Ph.D. degree in electrical engineering from the Institut National Polytechnique de Lorraine, Nancy, France, in 1994.

Since 1994, he has been a Researcher and a Teacher at the electrical engineering laboratory of the Polytechnic Military School, Algiers, Algeria. His current research interests are control of electrical drives and power electronics.



**Abderrezak Rezzoug** was born in 1948. He received the Electrical Engineer degree, Dr. Ing. diploma, and Ph.D. degree from ENSEM Institut National Polytechnique de Lorraine, Nancy, France, in 1972, 1979, and 1987, respectively.

He is currently a Professor in electrical engineering at the Université Henri Poincaré, Nancy. As a member of the Groupe de Recherche en Electrotechnique et Electronique de Nancy, Nancy, his main areas of research concern electrical machines, their identification, diagnostic and control, and superconducting applications.



## AUTHOR QUERIES

AUTHOR PLEASE ANSWER ALL QUERIES

AQ1 = “1972” was assumed as the author’s birth year. Please check if appropriate.

AQ2 = “1971” was assumed as the author’s birth year. Please check if appropriate.

AQ3 = Please provide the expanded form of the acronym “IUFM”.

AQ4 = “1974” was assumed as the author’s birth year. Please check if appropriate.

AQ5 = “1969” was assumed as the author’s birth year. Please check if appropriate.

AQ6 = “1948” was assumed as the author’s birth year. Please check if appropriate.

AQ7 = Please provide the expanded form of the acronym “ENSEM”.

Note: Figure citations were renumbered. The original sequence was 1-2-3-4-5-6-7-9-8.

END OF ALL QUERIES